

A Two-level Coordination Strategy for Distribution Network Balancing

Xueyuan Cui, *Student Member, IEEE*, Guangchun Ruan, *Member, IEEE*, François Vallée, *Member, IEEE*
Jean-François Toubeau, *Member, IEEE*, and Yi Wang, *Member, IEEE*

Abstract—Uncertain distributed energy resources and uneven load allocation cause the three-phase unbalance in distribution networks (DNs), which may harm the health of power equipment and increase the operational cost. There are emerging opportunities to balance three-phase DN with a number of power electronic devices installed in the system. In this paper, we propose a novel two-level coordination strategy to improve the network balancing performance, where soft open points (SOPs) and phase switch devices (PSDs) are hierarchically coordinated in the network. At the upper level, a new type of SOPs with the function of phase switching is designed to explore the cross-phase power transfer ability; at the lower level, PSDs are utilized to flexibly allocate individual loads to specific phases. The two-level coordination strategy is typically formulated as a mixed-integer nonlinear programming (MINLP) problem. To solve the model accurately and efficiently, we develop a successive linearization algorithm to approximate it to a mixed-integer linear programming (MILP) problem at each iteration. On this basis, we propose a heuristic time-independent fixing algorithm to further ease the computational burden by eliminating a large number of integer variables in the MILP problem. Numerical simulations are conducted to validate the effectiveness, accuracy, and efficiency of the proposed method.

Index Terms—Three-phase unbalance, soft open points, phase switch device, hierarchical control, successive linearization.

NOMENCLATURE

A. Indices and Sets

i, j	Indices of nodes.
α, β	Indices of phases.
t	Index of time slots.
m	Index of phase-switching periods.
$\mathcal{N}^+, \mathcal{N}$	Set of three-phase nodes with/without the root node in the network.
\mathcal{L}	Set of lines in the network.
\mathcal{N}^{SOP}	Set of node pairs (i, j) connected with two terminals of SOPs.

This work was supported in part by the National Key R&D Program of China (2022YFE0141200), in part by the National Natural Science Foundation of China (72242105), and in part by the Seed Fund for Basic Research for New Staff of The University of Hong Kong (202107185032). (*Corresponding author: Yi Wang.*)

Xueyuan Cui and Yi Wang are with the Department of Electrical and Electronic Engineering, The University of Hong Kong, Hong Kong SAR, China, and are also with The University of Hong Kong Shenzhen Institute of Research and Innovation, Shenzhen 518057, China.

Guangchun Ruan is with the Laboratory for Information & Decision Systems, Massachusetts Institute of Technology, Boston, MA 02139, USA.

François Vallée is with the Electrical Power Engineering Unit, University of Mons, 7000 Mons, Belgium.

Jean-François Toubeau is with the Energy Systems Integration & Modeling Group, KU Leuven, 3001 Leuven, Belgium.

Φ	Set of phases, defined as $\Phi := \{a, b, c\}$.
\mathcal{T}	Set of the operation period.
$\Omega_i^{\text{PY}}, \Omega_i^{\text{PN}}$	Set of single-phase users installed with/without PSDs in node i .
Ω^{DER}	Set of DERs (PV and WT) with installation nodes and phases.
Ω_i^{FL}	Set of users with responsive load in node i .

B. Parameters

\bar{S}_i^{S}	Capacity of PS-SOP connected to node i .
λ_i^{S}	Loss coefficient of PS-SOP in node i .
$N_j^{\text{S}}, N_{i,n}^{\text{PY}}$	Upper limit of phase switching number of the PS-SOP in node j and PSD installed with user n in node i .
c^{UNB}	Cost coefficient of unbalance level.
c^{LOSS}	Cost coefficient of network loss.
c^{CUR}	Cost coefficient of renewable curtailment.
c^{FL}	Cost coefficient of load alteration.
\bar{S}_α	Upper limit of apparent power injection of phase α in root node.
$\bar{V}_i^\alpha, \underline{V}_i^\alpha$	Upper/lower limit of voltage magnitude of phase α in node i .
V^{ref}	Reference voltage magnitude.
$\bar{I}_{ij}^{\alpha\alpha}$	Upper limit of current of phase $\alpha\alpha$ at line ij .
\bar{V}^{STD}	Upper limit of unbalance level in the network.
$\bar{P}_{i,\alpha,t}^{\text{PRE}}$	Forecasting value of active power generation of DERs (PV and WT) of phase α in node i at time t .
$\bar{S}_{i,\alpha}^{\text{DER}}$	Capacity of DERs of phase α in node i .
$\psi_{i,\alpha}^{\text{DER}}$	Upper limit of DER power factor of phase α in node i .
$P_{i,n,t}^{\text{D}}$	Active power demand of user n in node i at time t .
$Q_{i,n,t}^{\text{D}}$	Reactive power demand of user n in node i at time t .
$\bar{P}_{i,n,t}^{\text{DX}}$	Fixed part of responsive load of user n in node i at time t .
$\bar{P}_{i,n,t}^{\text{DFO}}$	Base part of the fully flexible load of user n in node i at time t .
$\psi_{i,n}^{\text{FL}}$	Maximum coefficient of flexible load of user n in node i .
$\mathbf{y}_{ij}, \mathbf{z}_{ij}$	Phase admittance and impedance matrix at line ij , satisfying $\mathbf{y}_{ij} = (\mathbf{z}_{ij})^{-1} \in \mathbb{C}^{3 \times 3}$.
M	Number of phase-switching periods in the whole operation period.

C. Decision Variables

$P_{i,\alpha,t}$	Active power injection of phase α in node i at time t .
$Q_{i,\alpha,t}$	Reactive power injection of phase α in node i at time t .
$V_{i,t}^\alpha$	Voltage magnitude of phase α in node i at time t .
$\theta_{i,t}^\alpha$	Voltage angle of phase α in node i at time t .
$P_{i,\alpha,t}^S$	Active power injection of PS-SOP connected to phase α of node i at time t .
$Q_{i,\alpha,t}^S$	Reactive power injection of PS-SOP connected to phase α in node i at time t .
$P_{i,\alpha,t}^{DER}$	Active power injection of DERs of phase α in node i at time t .
$Q_{i,\alpha,t}^{DER}$	Reactive power injection of DERs of phase α in node i at time t .
$P_{i,n,t}^{DFU}$	Upward flexible load of user n in node i at time t .
$P_{i,n,t}^{DFD}$	Downward flexible load of user n in node i at time t .
$\mu_{j,\phi,t}^S$	Binary variable $\{0, 1\}$ indicating whether the PS-SOP is connected as phase sequence ϕ in node j at time t .
$\mu_{i,n,\alpha,t}^{PY}$	Binary variable $\{0, 1\}$ indicating whether PSD installed with user n in node i is switched into phase α at time t .

D. State Variables

C^{OBJ}	The sum of costs in the objective.
C^{UNB}	The cost of unbalance level in the objective.
C^{LOSS}	The cost of network loss in the objective.
C^{CUR}	The cost of curtailment in the objective.
C^{FL}	The cost of load alteration in the objective.
$P_{i,\alpha,t}^{PL}$	Active power loss of PS-SOP connected to phase α in node i at time t .
$P_{i,\alpha,t}^{CUR}$	Active power curtailment of DERs (PV and WT) of phase α in node i at time t .
$P_{i,n,t}^{PDF}$	Fully flexible part of responsive load of user n in node i at time t .
$I_{ij,t}^{\alpha\alpha}$	Current magnitude of phase $\alpha\alpha$ at line ij at time t .
$\tilde{V}_{i,t}^{POS}$	Positive sequence voltage in node i at time t .
$\tilde{V}_{i,t}^{NEG}$	Negative sequence voltage in node i at time t .
$\tilde{V}_{i,t}^{ZER}$	Zero sequence voltage in node i at time t .
$\tilde{V}_{i,t}^\alpha$	Voltage of phase α in node i at time t , denoted as $\tilde{V}_{i,t}^\alpha = V_{i,t}^\alpha \angle \theta_{i,t}^\alpha$.

I. INTRODUCTION

UNCERTAIN distributed energy resources (DERs) and uneven load allocation make it challenging to mitigate three-phase unbalance in distribution networks (DNs) [1]. The unbalanced operational conditions are expected to have serious impacts on different levels [2]: for the main feeder at the root node, the unbalanced current injection reduces the available power capacity and increases the self-loss in the second side

of transformers; for the three-phase induction motors, the unbalanced voltage will induce vibrations and reduce the operational efficiency with the increasing reactive losses; for the three-phase-four-wire lines, the unbalanced power will cause extra losses on both the phase lines and neutral line [3].

Existing efforts to mitigate the unbalance in DNs can be roughly summarized into three categories. The first category is a static solution that consists in manually adjusting the connected phases of single-phase users. In [4], a current balancing method was proposed with phase identification, which adjusted users to another phase accordingly. Geographical Information Systems were utilized in [5] to identify the minimal number of phase connections for manual adjustment. Phase balancing performances of several heuristic algorithms (e.g., the greedy algorithm, exhaustive search, and backtracking algorithm) were tested and compared in [6]. The manual balancing method is manpower-intensive, so it is only possible for small-scale systems with a limited number of users.

The second category is to dynamically explore the balancing abilities of the existing power electronic devices in DNs, such as static var compensators (SVCs), step voltage regulators (SVRs), distributed generators (DGs), and soft open points (SOPs). The phase balancing performances of different devices were concluded and compared in [7]. Specifically, SVCs can provide capacitive or inductive currents between any two phases at the connection points. This feature was utilized in [8] to redistribute the current injection among three phases. SVRs can regulate the voltage magnitude via three-phase individual tap control. To mitigate voltage unbalance in the operation of active distribution networks (ADNs), SVRs were utilized in [9], [10] with the consideration of loss minimization. DGs can flexibly adjust the active or reactive power injection in the connected nodes for voltage unbalance mitigation. The optimal operation of ADNs involving voltage unbalance mitigation was proposed in [11], where the three-phase independent adjustment ability of DG inverters was utilized to balance individual voltage phases. In [12], a reactive power compensation strategy with distributed solar photovoltaic (PV) inverters was proposed for local voltage balancing. In [13], PV systems in multiple microgrids were centrally coordinated to mitigate the current and voltage unbalance at the same time. In [14], the independent per-phase control capability of three-phase DG inverters was fully explored to improve the network performance in loss reduction and phase balancing. In addition to the single network, the voltage unbalance was further considered in the interconnected DNs [15], where DGs were aggregated to provide more flexibilities in the optimal operation of ADNs. Instead of only balancing the voltage and current in the connected nodes, SOPs have enlightened a wider range of balancing capacities in DNs than SVCs and PV inverters. SOPs are generally installed to connect different nodes with a public direct current link, and they can transfer active power without limits of power flow equations [16]. The cross-node power transfer abilities were utilized in recent research for network balancing. Together with objectives of power loss reduction and voltage profile improvement, the load balancing performance of SOPs was preliminarily verified in [17] using a multi-objective operation model. In [18], [19],

TABLE I
LITERATURE COMPARISON FOR NETWORK BALANCING

Categories	Ref.	Characteristic			Object		Scale	
		Real-time control	Active power rephase	Reactive compensation	Voltage	Current	Inner node	Cross node
Manual adjustment	[4]–[6]		X			X	X	
SVCs	[8]	X	X			X	X	
SVRs	[9], [10]	X		X	X		X	
DGs	[11]–[14]	X	X	X	X		X	
SOPs	[17]–[21]	X	X	X	X	X		X
SOPs (Phase-changing)	[22], [23]	X	X	X	X			X
PSDs	[8], [25], [27]–[30]	X	X			X	X	
<i>Proposed method</i>	<i>/</i>	X	X	X	X	X	X	X

the voltage and current balancing abilities of SOPs were explored with the coordination of distributed generators. The robust optimization model was proposed in [20] to ensure the current balancing abilities of SOPs which fully considered the forecasting uncertainties of DERs generations. A new type of multi-terminal SOPs was proposed in [21], which was connected with electromechanical switches to increase the power transferred among feeders in DNs. Besides the flexible cross-node power transfer ability, the cross-phase power transfer of SOPs was first explored in [22], showing a significant improvement in load balancing compared with the regular SOPs. Furthermore, this phase changing ability was explored in multi-terminal SOPs [23], which improved the load balancing performance among a larger scale of nodes.

The third category is to design special phase switch devices (PSDs) for network balancing. PSDs are universally installed for dynamic allocation of single-phase users to specific phases [24]. In case that data measurement and communication were limited, the sensitivity of voltage unbalance to power injection was deduced in [25]–[27] to determine the local control strategies for PSDs within each node. However, the sensitivity formula can only be used when the phase voltage magnitudes and angles are weakly dependent. With network models and data measurements, the centralized method can determine the optimal balancing strategies while ensuring network security globally. In [28], a central load balancing model was formulated to optimize user phase connections by controlling PSDs efficiently. [29] showed that strategically selecting appropriate nodes for PSDs installation and load balancing can achieve comparable performance to the scenario where all nodes are installed with PSDs. Besides, an economic balancing method was studied in [30] by determining the optimal installation number of PSDs. PSDs are efficient for network balancing since they can be controlled in real-time. However, PSDs can only allocate user loads to one certain phase instead of distributing the user loads among three phases in a more fine-grained way. In addition, the balancing ability of PSDs is directly limited to the time-varying power consumption of connected users. To achieve the smoothing load balancing ability, a coordinated strategy with SVCs and PSDs was proposed in [8]. Since both SVCs and PSDs are installed within one node, the load-adjusting range is still limited in this node.

A summary of the related network balancing means is listed in Table I. When adopting various implementations

for network balancing, the decision-making process is generally determined by multi-period optimal power flow (OPF). To incorporate unbalance issues in OPF, a model-dependent impact assessment was performed within the multi-period OPF framework [31], with consideration of phase imbalances, neutral and ground wires, and load dependencies. Furthermore, to solve multi-period OPF in unbalanced DNs, Kron reduction was utilized in [32] to eliminate the neutral phase and determine the optimal control strategy. The possible multiple load-flow solutions in the presence of neutral conductors and groundings were analyzed in [33]. Besides, to reduce the computational time and complexity caused by the unbalance issue, an efficient solution algorithm was proposed in [34] for DER dispatch by decoupling the temporal relationship in the multi-period OPF.

According to the latest progress summarized above, we are able to identify two research gaps as follows: 1) Very few works explore the joint management of the inner-node phase switching and the cross-node power redistribution abilities for efficient network balancing, which is important for a larger balancing region with better balancing performance; 2) The existing phase-changing function of SOPs should be preset and cannot adapt to time-varying unbalance conditions, which is not flexible enough for more complex balancing scenarios.

To fill these gaps, we propose a novel two-level network balancing strategy where SOPs and PSDs are hierarchically coordinated to make full use of inner-node phase switching and cross-node power redistribution abilities at the network level. In this strategy, we design a new type of phase-switching soft open points (PS-SOPs) to further explore the network balancing functions of SOPs to achieve the real-time cross-phase power transfer ability.

This paper makes the following contributions:

- 1) **New strategy:** Propose a two-level network balancing strategy by coordinating SOPs and PSDs. In this strategy, PSDs flexibly allocate the user loads to different phase lines locally, while SOPs achieve cross-phase and cross-node power transfer to mitigate unbalance globally.
- 2) **New approach:** Develop a novel kind of PS-SOPs to achieve the real-time cross-phase power transfer function. Instead of the direct connection from the SOP terminal to the network node, we propose to install three PSDs between them, which can transfer active power among different phases by the corresponding on-

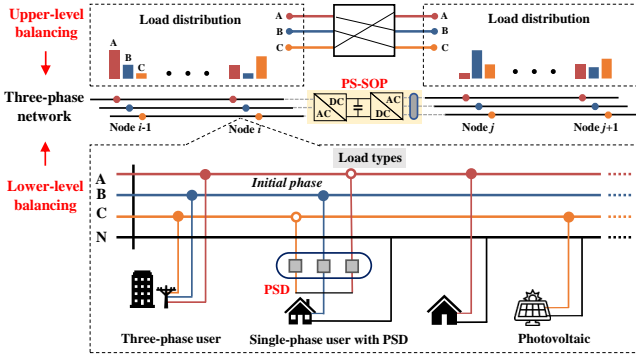


Fig. 1. Proposed two-level network balancing strategy.

off control of PSDs.

- 3) **New algorithm:** Formulate the network balancing strategy as a mixed-integer nonlinear programming (MINLP) problem. On this basis, we develop a successive linearization algorithm to approximate it to a mixed-integer linear programming (MILP) problem. We further propose a heuristic time-independent fixing algorithm to ease the computational burden by eliminating a large number of integer variables in the MILP problem.

The rest of this paper is organized as follows: Section II introduces the proposed network balancing strategy by coordinating PS-SOPs and PSDs. Section III provides details of the optimal coordination model, while Section IV presents the solution algorithm. Section V then conducts case studies to verify the effectiveness of the proposed method. Finally, Section VI draws the conclusion.

II. TWO-LEVEL NETWORK BALANCING STRATEGY

A two-level network balancing strategy is developed by hierarchically coordinating the proposed PS-SOPs with PSDs in DNs, where “two-level” refers to the coordination of both the upper-level and the lower-level balancing with different implementations. Fig. 1 shows the overview of the whole strategy. Here, the upper-level balancing is achieved by the real-time phase-switching functions of our designed PS-SOPs. The lower-level balancing is achieved by adjusting the phases of users installed with PSDs. Phase balancing functions at two levels are coordinated simultaneously. Action decisions of PSDs and PS-SOPs are implemented by receiving the control signals from the operation center. Operation principles of the upper-level and lower-level balancing are explained in the following subsections.

A. Upper-level Balancing With PS-SOPs

Three-phase SOPs are used to connect adjacent alternating current (AC) nodes within the network or among different networks. Among various kinds of topologies of SOPs, the back-to-back voltage source converters (VSCs)-based SOP [35] is widely utilized to participate in various network operation tasks (e.g., load balancing, power loss reduction, and voltage

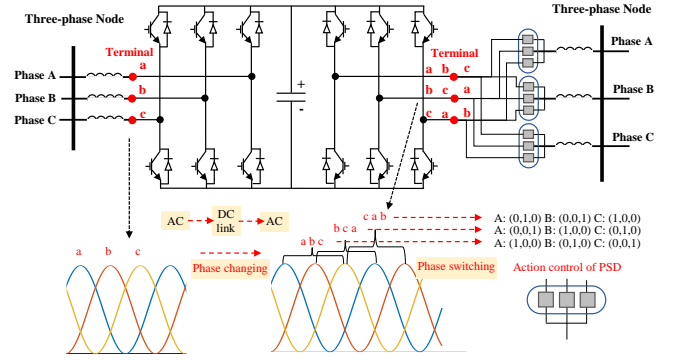


Fig. 2. Proposed topology and principle of phase-switching soft open points.

profile regulation), so this type of SOPs is studied in this work. In this type, a public direct current (DC) link is connected between two AC terminals. Both VSCs build the voltage waveforms under normal operation conditions, allowing full control of active power transfer through AC nodes and independent reactive power support.

Based on the basic topology of SOPs, we explore connecting three PSDs between one of the AC terminals and the corresponding three-phase node to achieve more flexible power transfer among different phases. The newly developed type is denoted as PS-SOPs, whose connection relationship and the phase switching principle are presented in Fig. 2. Each PSD is composed of three switching components, which connect the network node with all three ports of one terminal in SOPs. Through the decoupling DC link, the voltage waveforms experience a phase-changing process in the rectification or inversion stage, and thus the phase sequences of active power are different between two terminals (e.g., $a-b-c$ and $b-c-a$). The feasibility and rationality of the phase-changing function have been analyzed in [22]. In particular, by switching the action orders of PSDs w.r.t. the changed phase sequence, the active power can flow into the corresponding phase lines in DNs. Therefore, the phase-switching process can be achieved by the flexible and time-varying control of three connected switches. With the coordination of switch devices, this new ability is important to transfer the unbalanced load amounts among three phases across the connected nodes.

Denote that AC nodes i, j are connected with two terminals of the PS-SOP, and the terminal at node j is installed with the phase-switching function. Define Φ^S as the set of phase sequences, i.e., $\Phi^S := \{(abc), (bca), (cab)\}$, and take ϕ as the index for the candidate phase sequence, e.g., $\Phi_{\phi=1}^S = (abc)$, $\Phi_{1,1}^S = (abc)_1 = a$. For $\forall(i, j) \in \mathcal{N}^{\text{SOP}}, \forall t \in \mathcal{T}$, the phase-

switching power transfer process is formulated as

$$P_{i,a,t}^S + P_{i,a,t}^L + \sum_{\phi=1}^3 \mu_{j,\phi,t}^S (P_{j,\Phi_{\phi,1,t}^S}^S + P_{j,\Phi_{\phi,1,t}^L}^L) = 0 \quad (1a)$$

$$P_{i,b,t}^S + P_{i,b,t}^L + \sum_{\phi=1}^3 \mu_{j,\phi,t}^S (P_{j,\Phi_{\phi,2,t}^S}^S + P_{j,\Phi_{\phi,2,t}^L}^L) = 0 \quad (1b)$$

$$P_{i,c,t}^S + P_{i,c,t}^L + \sum_{\phi=1}^3 \mu_{j,\phi,t}^S (P_{j,\Phi_{\phi,3,t}^S}^S + P_{j,\Phi_{\phi,3,t}^L}^L) = 0 \quad (1c)$$

$$\sum_{\phi=1}^3 \mu_{j,\phi,t}^S = 1, \quad \mu_{j,\phi,t}^S \in \{0, 1\} \quad (1d)$$

where (1a)-(1c) represents the phase-switching process between nodes i and j ; (1d) represents the basic limit that one and only one phase sequence is determined.

Considering that too frequent phase-switching actions will cause extra costs and stability problems of PSDs [30], we limit the number of action times during each phase-switching period (i.e., the time period when limiting the action times of switch devices). For each phase-switching period ($\forall m = 1, 2, \dots, M$), the corresponding constraint is formulated as

$$\sum_{t \in \mathcal{T}_m} \sum_{\phi=1}^3 \frac{|\mu_{j,\phi,t}^S - \mu_{j,\phi,t-1}^S|}{2} \leq N_j^S, \quad \forall j \in \mathcal{N}^{\text{SOP}} \quad (2)$$

Besides, constraints of SOPs capacity and the active power loss in two terminals [36] are presented as

$$(P_{i,\alpha,t}^S)^2 + (Q_{i,\alpha,t}^S)^2 \leq (\bar{S}_i^S)^2, \quad \forall i \in \mathcal{N}^{\text{SOP}} \quad (3a)$$

$$P_{i,\alpha,t}^L = \lambda_i^S |P_{i,\alpha,t}^S|, \quad \forall i \in \mathcal{N}^{\text{SOP}} \quad (3b)$$

B. Lower-level Balancing With PSDs

As a type of mature product applied for unbalance mitigation, PSDs have been widely adopted in real-world trials as well as engineering applications. Simulation work was conducted in [24] to verify the performance of voltage mitigation and the dynamic stability during the phase switching process; detailed tests in the real-world trial [37] verified that PSDs could work normally and ensure voltage and current qualities by detecting zero-crossing points of current waveforms; furthermore, the practical products and the real-world projects [38] showed an acceptable cost and guaranteed power quality in engineering applications.

In practice, one terminal of the PSD is installed with three switching devices to connect each phase line of the network, and another terminal is connected to the user. After the PSD controller receives the action signals from operators, the switching devices will conduct the rephasing action with the uninterrupted power supply [24].

In the specific settings, the single-phase users at node i can be classified into two sets: with PSDs installation Ω_i^{PY} , or without PSDs installation $\Omega_i^{\text{PN}} = \{\Omega_{i,a}^{\text{PN}}, \Omega_{i,b}^{\text{PN}}, \Omega_{i,c}^{\text{PN}}\}$. The

power injection of node i with PSDs actions in the lower-level balancing is formulated as

$$P_{i,\alpha,t}^D + \mathbf{i}Q_{i,\alpha,t}^D = \sum_{n \in \Omega_{i,\alpha}^{\text{PN}}} (\bar{P}_{i,n,t}^D + \mathbf{i}\bar{Q}_{i,n,t}^D) + \sum_{n \in \Omega_i^{\text{PY}}} \mu_{i,n,\alpha,t}^{\text{PY}} (\bar{P}_{i,n,t}^D + \mathbf{i}\bar{Q}_{i,n,t}^D), \quad \forall i \in \mathcal{N}, \forall \alpha \in \Phi_i, \forall t \quad (4a)$$

$$\sum_{\alpha \in \Phi_i} \mu_{i,n,\alpha,t}^{\text{PY}} = 1, \quad \forall i \in \mathcal{N}, \forall n \in \Omega_i^{\text{PY}}, \forall t \quad (4b)$$

$$\mu_{i,n,\alpha,t}^{\text{PY}} \in \{0, 1\}, \quad \forall i \in \mathcal{N}, \forall n \in \Omega_i^{\text{PY}}, \forall \alpha \in \Phi_i, \forall t \quad (4c)$$

where (4a) is the power injection including the phase-fixed power from Ω_i^{PN} and the phase-switchable power from Ω_i^{PY} ; similar with (1d), the basic action of each PSD is limited in (4b) to prevent short-circuiting on phase lines, with the binary variables introduced in (4c).

Similarly, the action times of PSDs in each \mathcal{T}_m ($\forall m = 1, 2, \dots, M$) during the entire period is limited as

$$\sum_{t \in \mathcal{T}_m} \sum_{\alpha \in \Phi_i} \frac{|\mu_{i,n,\alpha,t}^{\text{PY}} - \mu_{i,n,\alpha,t-1}^{\text{PY}}|}{2} \leq N_{i,n}^{\text{PY}}, \quad \forall i \in \mathcal{N}, \forall n \in \Omega_i^{\text{PY}} \quad (5)$$

Remark 1: In the lower-level balancing process, the switching decisions of PSDs are always different whether coordinating with PS-SOPs or not. Without the upper-level balancing process, the action objective of PSDs is to minimize the unbalance level within the installed node, which, however, can not always ensure the global balance conditions in DNs. So the proposed coordinated strategy is not decoupled, and we cannot optimize the action decisions of PSDs and power transfer of PS-SOPs independently but have to optimize it together to obtain the global balancing results.

III. OPTIMAL COORDINATION MODEL

A. Objective

In the proposed coordination model, the objective function (6a) for network balancing in the operation period is composed of the following parts: unbalance level cost (6b), network loss cost (6c), renewable curtailment cost (6d), and load alteration cost (6e).

$$C^{\text{OBJ}} = C^{\text{UNB}} + C^{\text{LOSS}} + C^{\text{CUR}} + C^{\text{FL}} \quad (6a)$$

$$C^{\text{UNB}} = c^{\text{UNB}} \sum_{t \in \mathcal{T}} f_t^{\text{UNB}} \quad (6b)$$

$$C^{\text{LOSS}} = c^{\text{LOSS}} \sum_{t \in \mathcal{T}} \sum_{\alpha \in \Phi_i} \left(\sum_{i \in \mathcal{N}^+} P_{i,\alpha,t} + \sum_{i \in \mathcal{N}^{\text{SOP}}} P_{i,\alpha,t}^L \right) \quad (6c)$$

$$C^{\text{CUR}} = c^{\text{CUR}} \sum_{t \in \mathcal{T}} \sum_{(i,\alpha) \in \Omega^{\text{DER}}} P_{i,\alpha,t}^{\text{CUR}} \quad (6d)$$

$$C^{\text{FL}} = c^{\text{FL}} \sum_{t \in \mathcal{T}} \sum_{i \in \mathcal{N}} \sum_{n \in \Omega_i^{\text{FL}}} (P_{i,n,t}^{\text{DFU}} + P_{i,n,t}^{\text{DFD}}) \quad (6e)$$

Three-phase unbalance will bring extra operation costs in DNs, and some related research has focused on how to quantify the operation cost or asset reinforcement cost caused by voltage unbalance [2], [39]. Besides, extra costs on network

loss can be also caused by current unbalance levels. We demonstrate the current unbalance-related costs in Appendix-A. Thus, more recent researches begin to minimize the unbalance levels in the operation objective functions, which mainly refer to the branch power/current from the root node [8] and voltage phases at each node [19], [40] in DNs. We formulate the objective of unbalance with four parts, including the active and reactive power injection at the root node ($f_{P,t}^{\text{UNB}}, f_{Q,t}^{\text{UNB}}$), and voltage magnitude ($f_{V,t}^{\text{UNB}}$) and angle ($f_{\theta,t}^{\text{UNB}}$) at each node. The objective to minimize the unbalance level is formulated as

$$f_t^{\text{UNB}} = \xi_1(f_{P,t}^{\text{UNB}} + f_{Q,t}^{\text{UNB}}) + \xi_2(f_{V,t}^{\text{UNB}} + f_{\theta,t}^{\text{UNB}}) \quad (7a)$$

$$f_{P,t}^{\text{UNB}} = 3P_{0,\max,t} - (P_{0,a,t} + P_{0,b,t} + P_{0,c,t}) \quad (7b)$$

$$f_{Q,t}^{\text{UNB}} = 3Q_{0,\max,t} - (Q_{0,a,t} + Q_{0,b,t} + Q_{0,c,t}) \quad (7c)$$

$$f_{V,t}^{\text{UNB}} = \sum_{i \in \mathcal{N}} 3V_{i,t}^{\max} - (V_{i,t}^a + V_{i,t}^b + V_{i,t}^c) \quad (7d)$$

$$f_{\theta,t}^{\text{UNB}} = \sum_{i \in \mathcal{N}} (|\theta_{i,t}^a - \theta_{i,t}^b - 120^\circ| + |\theta_{i,t}^b - \theta_{i,t}^c - 120^\circ| + |\theta_{i,t}^c - \theta_{i,t}^a - 120^\circ|) \quad (7e)$$

where ξ_1, ξ_2 are coefficients to scale power and voltage unbalance ranges; $P_{0,\max,t}$ and $Q_{0,\max,t}$ are the maximal active and reactive power injection of three phases in the root node at time t ; $V_{i,t}^{\max}$ is the maximal voltage magnitude of three phases in node i at time t . The effectiveness of the proposed method for unbalance representation is explained in Appendix-B. The application advantages are concluded as 1) the new indexes are similarly effective with sequence voltage components to represent unbalance levels; 2) the new indexes are linear and can be easily incorporated into the optimization model.

B. Constraints

Besides the operation principles of PS-SOPs and PSDs, the other constraints considering the three-phase power flow, secure operation, and power injections are presented as follows (the time t label is ignored for simplicity).

1) *Power flow equations*: We take the common three-phase-four-wire distribution networks for illustration. To integrate the neutral line loss into the phase line loss, Kron Reduction [41] is first utilized to reduce the original 4×4 network impedance matrix as \mathbf{z}_{ij} with the size of 3×3 . Taking the power injection, node voltage, and node phase as variables, and considering the mutual inductance and interphase capacitance, the bus injection model (BIM)-based three-phase power flow equations are formulated as:

$$P_{i,\alpha} = \sum_{j \in \mathcal{N}^+} \sum_{\beta \in \Phi_i} V_i^\alpha V_j^\beta \left(G_{ij}^{\alpha\beta} \cos \theta_{ij}^{\alpha\beta} + B_{ij}^{\alpha\beta} \sin \theta_{ij}^{\alpha\beta} \right) \quad (8a)$$

$$Q_{i,\alpha} = \sum_{j \in \mathcal{N}^+} \sum_{\beta \in \Phi_i} V_i^\alpha V_j^\beta \left(G_{ij}^{\alpha\beta} \sin \theta_{ij}^{\alpha\beta} - B_{ij}^{\alpha\beta} \cos \theta_{ij}^{\alpha\beta} \right) \quad (8b)$$

$$\forall i \in \mathcal{N}^+, \forall \alpha \in \Phi_i$$

where $\theta_{ij}^{\alpha\beta} = \theta_i^\alpha - \theta_j^\beta$ is the angle difference between phase α in node i and phase β in node j ; $G_{ij}^{\alpha\beta}$ and $B_{ij}^{\alpha\beta}$ are the real

part and the imaginary part of the node admittance $\tilde{Y}_{ij}^{\alpha\beta} = G_{ij}^{\alpha\beta} + \mathbf{i}B_{ij}^{\alpha\beta}$, which is defined as

$$\tilde{Y}_{ij}^{\alpha\beta} = \begin{cases} -\tilde{y}_{ij}^{\alpha\beta}, & \text{if } j \neq i \\ \tilde{y}_{ii}^{\alpha\beta} + \sum_{k \in \mathcal{N}^+, k \neq i} \tilde{y}_{ik}^{\alpha\beta}, & \text{if } j = i \end{cases} \quad (9)$$

$$\forall i, j \in \mathcal{N}^+, \forall \alpha, \beta \in \{a, b, c\}$$

2) *Power injection limits*: The apparent power transfer from the upper grid connected with the root node satisfies the upper limit as

$$P_{0,\alpha,t}^2 + Q_{0,\alpha,t}^2 \leq \bar{S}_\alpha^2, \forall \alpha \in \Phi_0, \forall t \in \mathcal{T} \quad (10)$$

3) *Voltage magnitude limits*: All the node voltage magnitudes are limited within a normal range for the secure operation of DNs, which is shown as

$$\underline{V}_i^\alpha \leq V_{i,t}^\alpha \leq \bar{V}_i^\alpha, \forall i \in \mathcal{N}, \forall \alpha \in \Phi_i, \forall t \in \mathcal{T} \quad (11)$$

In particular, the phase voltage in the root node is assumed to be fixed as a standard value. Note that different bound conditions are feasible and a commonly assumed one [8], [19] is chosen in our case.

$$[\tilde{V}_{0,t}^a, \tilde{V}_{0,t}^b, \tilde{V}_{0,t}^c] = [V^{\text{ref}}, V^{\text{ref}} \angle -120^\circ, V^{\text{ref}} \angle 120^\circ] \quad (12)$$

4) *Line thermal limits*: The thermal capacity of each phase line in the distribution network is presented as

$$|I_{ij,t}^{\alpha\alpha}|^2 = |\tilde{y}_{ij}^{\alpha\alpha}|^2 ((V_{i,t}^\alpha)^2 + (V_{j,t}^\alpha)^2 - 2V_{i,t}^\alpha V_{j,t}^\alpha \cos \theta_{ij,t}^{\alpha\alpha}) \leq |\bar{I}_{ij}^{\alpha\alpha}|^2, \forall \alpha \in \{a, b, c\}, \forall ij \in \mathcal{L}, \forall t \in \mathcal{T} \quad (13)$$

5) *Voltage unbalance limits*: To limit the voltage unbalance level within the standard requirements [42], positive, negative, and zero sequence voltage components are deduced, and the negative sequence component is limited as follows (for $\forall i \in \mathcal{N}, \forall t \in \mathcal{T}$).

$$\left| \frac{\tilde{V}_{i,t}^{\text{NEG}}}{\tilde{V}_{i,t}^{\text{POS}}} \right| \leq \bar{V}^{\text{STD}} \quad (14a)$$

$$\tilde{V}_{i,t}^{\text{POS}} = \frac{1}{3} \left(\tilde{V}_{i,t}^a + e^{\mathbf{i}120^\circ} \tilde{V}_{i,t}^b + e^{\mathbf{i}240^\circ} \tilde{V}_{i,t}^c \right) \quad (14b)$$

$$\tilde{V}_{i,t}^{\text{NEG}} = \frac{1}{3} \left(\tilde{V}_{i,t}^a + e^{\mathbf{i}240^\circ} \tilde{V}_{i,t}^b + e^{\mathbf{i}120^\circ} \tilde{V}_{i,t}^c \right) \quad (14c)$$

$$\tilde{V}_{i,t}^{\text{ZER}} = \frac{1}{3} \left(\tilde{V}_{i,t}^a + \tilde{V}_{i,t}^b + \tilde{V}_{i,t}^c \right) \quad (14d)$$

6) *DER operation*: Two kinds of DERs including PV systems and wind turbines (WTs) are taken as distributed generator units. They are also responsible for voltage regulation in power connection points by generating or absorbing reactive power [43]. Denote that DERs are installed with nodes and phases $(i, \alpha) \in \Omega^{\text{DER}}$, ($\text{DER} = \{\text{PV}, \text{WT}\}$), the active and reactive power generation relationship at each time t is represented as

$$P_{i,\alpha,t}^{\text{DER}} + P_{i,\alpha,t}^{\text{CUR}} = \bar{P}_{i,\alpha,t}^{\text{PRE}} \quad (15a)$$

$$P_{i,\alpha,t}^{\text{DER}} \geq 0, P_{i,\alpha,t}^{\text{CUR}} \geq 0 \quad (15b)$$

$$(P_{i,\alpha,t}^{\text{DER}})^2 + (Q_{i,\alpha,t}^{\text{DER}})^2 \leq (\bar{S}_{i,\alpha}^{\text{DER}})^2 \quad (15c)$$

$$|Q_{i,\alpha,t}^{\text{DER}}| \leq P_{i,\alpha,t}^{\text{DER}} \tan \psi_{i,\alpha}^{\text{DER}} \quad (15d)$$

In the actual dispatch period, the active or reactive power generation can be flexibly adjusted by the requirement of load demand or voltage regulation [44], [45]. The DER schedulings in DNs are determined in day-ahead dispatch in our work.

7) *Responsive loads*: In the “smart grid” operation, the consumer loads can be flexibly adjusted in some scenarios (e.g., demand response). We consider the most common case that the original load is split into fixed and fully flexible parts [31]. For $\forall n \in \Omega_i^{\text{FL}}, \forall i \in \mathcal{N}, \forall t \in \mathcal{T}$, the responsive load of each consumer is defined as

$$P_{i,n,t}^{\text{D}} = \bar{P}_{i,n,t}^{\text{DX}} + P_{i,n,t}^{\text{DF}} \quad (16a)$$

$$P_{i,n,t}^{\text{DF}} = \bar{P}_{i,n,t}^{\text{DFU}} + P_{i,n,t}^{\text{DFD}} - P_{i,n,t}^{\text{DFD}} \quad (16b)$$

$$0 \leq P_{i,n,t}^{\text{DFU}}, P_{i,n,t}^{\text{DFD}} \leq \psi_{i,n}^{\text{FL}} \bar{P}_{i,n,t}^{\text{DFO}} \quad (16c)$$

where (16a) differentiates the fixed and fully flexible parts of responsive load; (16b) and (16c) indicate that the flexible part consists of the upward and the downward load alteration.

C. Optimization Model

Given the above objective function and constraints, the optimization problem to coordinate PS-SOPs and PSDs can be formulated as

$$\begin{aligned} \mathcal{P}_1 : \min (6) \\ \text{s.t. (1) - (5), (8), (10) - (15); } \forall t \in \mathcal{T} \end{aligned} \quad (17)$$

It can be seen that only constraints (2) and (5) are time-coupling in each phase-switching period \mathcal{T}_m , while other constraints are time-independent. So we can decouple the original problem into M subproblems, and solve each $\mathcal{P}_{1,m}, \forall t \in \mathcal{T}_m$ successively to simplify the solving process. Because integer variables (e.g., $\mu^{\text{S}}, \mu^{\text{PY}}$) and non-linear constraints (e.g., (1a)-(1c), (3a), (8), (15d)) are introduced in the original problem, it is a mixed-integer nonlinear programming (MINLP) problem. We claim that the proposed model is applied to networks with all three-phase laterals and nodes, and the unbalanced three-phase network including single-phase or two-phase laterals [46]–[48] is not in our research scope.

IV. SOLUTION ALGORITHM

A. Solution Framework

The original model of the proposed two-level coordination strategy is difficult to be solved mainly because of the non-convex power flow equations and the time-coupling limits on the action decisions of PSDs. It is necessary to formulate an accurate and efficient solution method to tackle computational problems. For the first issue, linearization methods are proposed to approximate the three-phase power flow, however, most of them are with balancing assumptions [46], including that the angle difference of the different phases is balanced and near 120° , or the per unit voltage magnitude is equal to 1. Linearization methods with such assumptions are essentially contradictory with the features of unbalanced DNs. They will cause unacceptable errors when used for approximation of \mathcal{P}_1 . For the second issue, the time-coupling relationship of action times increases the computational complexity of each $\mathcal{P}_{1,m}$.

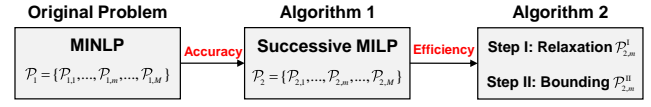


Fig. 3. Framework of solution algorithms.

The computation time is extended due to the longer phase-switching periods, more action times, and higher installation ratios of PSDs.

We propose a solution framework to cover the above challenges, which is explained in Fig. 3. In particular, we reformulate \mathcal{P}_1 as a MILP-based problem to solve it more accurately. Without assumptions on strict balance conditions and not sensitive to the initialization, the proposed method can find the suboptimal solution with guarantees of convergence. Furthermore, to speed up the solving efficiency, we propose a time-independent fixing algorithm to decouple the time relationship and find an accurate solution.

B. Successive Linearization Algorithm

1) *Linearization of power flow equations*: Ignoring the time index t and taking (8a) for illustration, the active power flow can be approximated by using Taylor series expansion and omitting the second and higher order terms as

$$P_{i,\alpha} \approx P_{i,\alpha}(0) + \sum_{j \in \mathcal{N}^+} \sum_{\beta \in \Phi_i} \frac{\partial P}{\partial V_j^\beta} (V_j^\beta - V_j^\beta(0)) + \frac{\partial P}{\partial \theta_j^\beta} (\theta_j^\beta - \theta_j^\beta(0)) \quad (18)$$

where $V(0)$, $\theta(0)$, and $P(0)$ are the initial variable values.

We can formulate the successive linearization equation in a matrix style, and define the Jacobian matrix \mathbf{J} containing all the Partial derivative results as

$$\mathbf{J} = \begin{bmatrix} \mathbf{J}_{PV} & \mathbf{J}_{P\theta} \\ \mathbf{J}_{QV} & \mathbf{J}_{Q\theta} \end{bmatrix} = \begin{bmatrix} \frac{\partial \mathbf{P}}{\partial \mathbf{V}} & \frac{\partial \mathbf{P}}{\partial \boldsymbol{\theta}} \\ \frac{\partial \mathbf{Q}}{\partial \mathbf{V}} & \frac{\partial \mathbf{Q}}{\partial \boldsymbol{\theta}} \end{bmatrix} \quad (19)$$

The size of \mathbf{J} is $6|\mathcal{N}^+| \times 6|\mathcal{N}^+|$, and two examples of matrix elements are given as

$$\begin{aligned} \mathbf{J}_{PV}(1, 1) &= \frac{\partial P_{1,a}}{\partial V_1^a} = V_1^a G_{11}^{aa} \\ &+ \sum_{j \in \mathcal{N}^+} \sum_{\beta \in \Phi_i} V_j^\beta \left(G_{ij}^{\alpha\beta} \cos \theta_{ij}^{\alpha\beta} + B_{ij}^{\alpha\beta} \sin \theta_{ij}^{\alpha\beta} \right) \end{aligned} \quad (20)$$

$$\begin{aligned} \mathbf{J}_{P\theta}(1, 1) &= \frac{\partial P_{1,a}}{\partial \theta_1^a} = -V_1^a V_1^a B_{11}^{aa} \\ &+ \sum_{j \in \mathcal{N}^+} \sum_{\beta \in \Phi_i} V_i^\alpha V_j^\beta \left(B_{ij}^{\alpha\beta} \cos \theta_{ij}^{\alpha\beta} - G_{ij}^{\alpha\beta} \sin \theta_{ij}^{\alpha\beta} \right) \end{aligned} \quad (21)$$

Finally, the k^{th} iteration in the successive linearization algorithm is presented as

$$\begin{bmatrix} \mathbf{P}(k+1) \\ \mathbf{Q}(k+1) \end{bmatrix} = \mathbf{J}(k) \cdot \begin{bmatrix} \mathbf{V}(k+1) - \mathbf{V}(k) \\ \boldsymbol{\theta}(k+1) - \boldsymbol{\theta}(k) \end{bmatrix} + \begin{bmatrix} \mathbf{P}(k) \\ \mathbf{Q}(k) \end{bmatrix} \quad (22)$$

2) *Linearization of other nonlinear constraints:* The quadratic constraints ((3a), (10), and (15c)) with circle regions are approximated by the piecewise linear modeling with the convex regular L -side polygon [49], which is shown as

$$P^2 + Q^2 \leq \bar{S}^2 \Leftrightarrow \begin{cases} \left[\sin\left(\frac{2\pi}{L}l\right) - \sin\left(\frac{2\pi}{L}(l-1)\right) \right] P + \\ \left[\cos\left(\frac{2\pi}{L}l\right) - \cos\left(\frac{2\pi}{L}(l-1)\right) \right] Q \leq \bar{S} \times \sin\frac{2\pi}{L} \\ l = 1, 2, \dots, L \end{cases} \quad (23)$$

where l is the index representing each edge of the polygon. Although this kind of constraint can be processed by some existing solvers, it can be incorporated into more applicable cases with indiscernible errors after linearization.

Constraints with absolute variables ((2), (3b), (5), and (7e)) or products of the binary and continuous variables ((1a)-(1c)) are reformulated by big M method [8] with a sufficiently large number M_{big} . The general reformulation process is given as

$$z = |y| \Leftrightarrow \begin{cases} y \leq z \leq y + M_{\text{big}}\delta_1 \\ -y \leq z \leq -y + M_{\text{big}}\delta_2 \\ \delta_1, \delta_2 \in \{0, 1\}, \delta_1 + \delta_2 = 1 \end{cases} \quad (24)$$

$$\begin{cases} z = xy \\ x \in \{0, 1\} \end{cases} \Leftrightarrow \begin{cases} y - (1-x)M_{\text{big}} \leq z \\ y + (1-x)M_{\text{big}} \geq z \\ -xM_{\text{big}} \leq z \leq xM_{\text{big}} \end{cases} \quad (25)$$

For the line thermal constraint (13), we suppose the angle difference between adjacent nodes can be ignored, then the nonlinear term is approximated as

$$\begin{aligned} |I_{ij}^{\alpha\alpha}|^2 &\approx |\tilde{y}_{ij}^{\alpha\alpha}|^2 ((V_i^\alpha)^2 + (V_j^\alpha)^2 - 2V_i^\alpha V_j^\alpha) \\ &= |\tilde{y}_{ij}^{\alpha\alpha}|^2 (V_i^\alpha - V_j^\alpha)^2 \end{aligned} \quad (26)$$

So the constraint is transformed as

$$|V_i^\alpha - V_j^\alpha| \leq |\tilde{I}_{ij}^{\alpha\alpha}| / |\tilde{y}_{ij}^{\alpha\alpha}|, \forall \alpha \in \{a, b, c\}, \forall ij \in \mathcal{L} \quad (27)$$

which can be further processed by (24).

For the unbalance constraint (14), we first approximate the real part $V_{\text{re}}^{\text{NEG}}$ and the imaginary part $V_{\text{im}}^{\text{NEG}}$ of the negative sequence voltage component with Taylor series expansion as

$$\tilde{V}_i^{\text{NEG}} = V_{\text{re}}^{\text{NEG}} + \mathbf{i}V_{\text{im}}^{\text{NEG}} \quad (28a)$$

$$V_{\text{re}}^{\text{NEG}} \approx \sum_{\alpha \in \Phi} \frac{\partial V_{\text{re}}^{\text{NEG}}}{\partial V^\alpha} (V^\alpha - V^\alpha(0)) + \sum_{\beta \in \Phi} \frac{\partial V_{\text{re}}^{\text{NEG}}}{\partial \theta^\beta} (\theta^\beta - \theta^\beta(0)) \quad (28b)$$

$$V_{\text{im}}^{\text{NEG}} \approx \sum_{\alpha \in \Phi} \frac{\partial V_{\text{im}}^{\text{NEG}}}{\partial V^\alpha} (V^\alpha - V^\alpha(0)) + \sum_{\beta \in \Phi} \frac{\partial V_{\text{im}}^{\text{NEG}}}{\partial \theta^\beta} (\theta^\beta - \theta^\beta(0)) \quad (28c)$$

where we take the balanced state ($V = 1.0$ p.u., $[\theta^a, \theta^b, \theta^c] = [0^\circ, -120^\circ, 120^\circ]$, $\tilde{V}^{\text{NEG}}(0) = 0$) as initial values.

By assuming $V^{\text{POS}} = 1 \angle 0^\circ$, the constraint (14a) can be approximated as

$$(V_{\text{re}}^{\text{NEG}})^2 + (V_{\text{im}}^{\text{NEG}})^2 \leq (\bar{V}^{\text{STD}})^2 \quad (29)$$

which can be further processed by (23).

3) *Final model:* After linearization, the original problem is transformed into the MILP problem as

$$\begin{aligned} \mathcal{P}_2 : \min (6) \\ \text{s.t. (1) - (5), (10) - (15), (22) - (25); } \forall t \in \mathcal{T} \end{aligned} \quad (30)$$

Similarly, we can decouple the whole operation period \mathcal{T} into M phase-switching periods and solve each $\mathcal{P}_{2,m}$ successively. Furthermore, in Algorithm 1, we propose an iteration algorithm to solve $\mathcal{P}_{2,m}$ and find the optimal solution of original $\mathcal{P}_{1,m}$. It should be noted that the solving method in Algorithm 1 is presented in the arbitrary period \mathcal{T}_m but can be equivalently used for the entire period. Solving the MILP problems iteration by iteration is a computationally effective way to avoid errors due to the approximation and initial point settings, and the adoption of constraints (31) is beneficial to limit the searching region and accelerate the convergence.

Discussion: It should be noted that the feasibility of the successive optimization process does not rely on the rank conditions of the Jacobian matrix \mathbf{J} in (19). There is some related research on the existence and uniqueness of power flow solutions, including the formal analysis [50], [51] and the possible way to ensure the uniqueness conditions [52]. Unlike the power flow calculation, the OPF model mainly focuses on how to find the optimal solution given the feasible region in each iteration, and convergence is more highly emphasized in the successive algorithm. Besides, other related research also utilized the Jacobian matrix for power flow calculation [52]–[54] or sensitivity analysis [55], [56]. On this basis, we propose the successive algorithm to determine the optimal solution by reducing the approximation errors iteratively.

C. Time-independent Fixing Algorithm

The proposed method to improve the computational efficiency is explained in Algorithm 2. It includes two steps: **Step I** performs a *conditional relaxation* for the original problem. It drops the time-coupling constraints (2) and (5) so that the problem is fully time-independent. However, computational complexities and solution errors will increase to recover the feasible solution if too many PSDs violate the action limits. Therefore, a penalty term on action times at each time is added to the objective function. Based on the conditional relaxation result, some action decisions of partial PSDs are within the phase-switching period limit while others are not. **Step II** fixes the action decisions of the former group of PSDs and re-optimizes to *bound* the optimal action decisions of the latter ones. By reducing the ratio of PSDs to be optimized, the computation time can be largely reduced.

Remark 1: In **Step I**, the aim of conditional relaxation is to decouple the time-dependent constraints and limit the number of PSDs violating action constraints. First, an appropriate setting of the penalty term in F_t^I is important to achieve the aim. Considering that the corresponding coefficient ξ^{PEN} can not be determined in closed form [57], some common search techniques (e.g., Fibonacci searching [58]) can be adopted to determine it. Besides, a suitable number of PSDs in $\Omega_{\text{ao}}^{\text{PY}}$ is important for the tradeoff between the optimization time and the relaxation error. For example, results with an empty set

Algorithm 1 Successive Linear Programming

Input: Initial variables $\mathbf{V}(0), \boldsymbol{\theta}(0)$; convergence threshold $\varepsilon_1, \varepsilon_2$; initial iteration index $k = 0$; parameters for problem $\mathcal{P}_{1,m}$.

Output: Optimal variables $[\mathbf{P}^*, \mathbf{Q}^*, \mathbf{V}^*, \boldsymbol{\theta}^*]$ and objective solution F^* for problem $\mathcal{P}_{1,m}$.

- 1: **repeat**
- 2: Calculate (22) with input $\mathbf{V}(k), \boldsymbol{\theta}(k)$;
- 3: Formulate problem $\mathcal{P}_{2,m}$ with constraints on the iteration step size:

$$\begin{aligned} \max\{|\mathbf{V} - \mathbf{V}(k)|\} &\leq \frac{1}{2^k} \\ \max\{|\boldsymbol{\theta} - \boldsymbol{\theta}(k)|\} &\leq \frac{1}{2^k} \end{aligned} \quad (31)$$

- 4: Solve $\mathcal{P}_{2,m}$ with (31) by MILP solvers and update the variable vector $[\mathbf{P}(k+1), \mathbf{Q}(k+1), \mathbf{V}(k+1), \boldsymbol{\theta}(k+1)]$ as well as the objective value $F(k+1)$;
- 5: Update iteration index $k = k + 1$;
- 6: Calculate power flow equation (8) with $\mathbf{V}(k+1), \boldsymbol{\theta}(k+1)$ to determine the actual power value $\mathbf{P}_{\text{PF}}(k+1), \mathbf{Q}_{\text{PF}}(k+1)$;
- 7: Calculate the iteration errors $\varepsilon_{\text{obj}}, \varepsilon_p$, and ε_q as:

$$\begin{aligned} \varepsilon_{\text{obj}}(k+1) &= \frac{|F(k+1) - F(k)|}{F(k)} \\ \varepsilon_p(k+1) &= \max\{|\mathbf{P}_{\text{PF}}(k+1) - \mathbf{P}(k+1)|\} \\ \varepsilon_q(k+1) &= \max\{|\mathbf{Q}_{\text{PF}}(k+1) - \mathbf{Q}(k+1)|\} \end{aligned} \quad (32)$$

- 8: **until** $\varepsilon_{\text{obj}}(k+1) \leq \varepsilon_1$ and $\max\{\varepsilon_p(k+1), \varepsilon_q(k+1)\} \leq \varepsilon_2$
-

of $\Omega_{\text{ao}}^{\text{PY}}$ (i.e., no PSDs violate constraints) will reduce the total computational time but result in the less accurate solution with a large relaxation error. An empirically better setting shows that action decisions of a small proportion of PSDs are out of limit. An ideal range for the iteration termination condition is set as $|\Omega_{\text{ao}}^{\text{PY}}| \leq 0.3|\Omega^{\text{PY}}|$ in **STEP I**.

Remark 2: The essence of the proposed algorithm to reduce the solving complexity is to decouple the time-dependent relationship. **Step I** and **Step II** have achieved this target in different ways. **Step I** directly drops the time-coupling constraints and thus solves the problem every single time. With a conditional relaxation result from **Step I**, all the constraint-violating decisions of PSDs can meet the action limits in **Step II**, and the reduced variable number of PSDs improves the computational efficiency greatly.

V. CASE STUDY

A. Simulation Setup

As shown in Fig. 4, the modified three-phase IEEE-33 distribution network is adopted to verify the effectiveness of the proposed method. The network parameters are obtained in [19]. Load data of low-voltage users in ISSDA dataset [59] are distributed in each three-phase load node, with 24h operation period and 1h time interval. As the main DER types, 10 PV systems and 1 wind turbine are located in the network. In Fig. 4, a certain proportion of users are installed with PSDs

Algorithm 2 Time-independent Fixing Procedure

Input: Total set of PSDs Ω^{NY} ; initial phase settings of PSDs $\boldsymbol{\mu}^{\text{PY}}(0)$; parameters for problem $\mathcal{P}_{2,m}$.

Output: Feasible variables $[\mathbf{P}^{\text{II}}, \mathbf{Q}^{\text{II}}, \mathbf{V}^{\text{II}}, \boldsymbol{\theta}^{\text{II}}]$ and objective function F^{II} for problem $\mathcal{P}_{2,m}$.

STEP I: Conditional Relaxation

- 1: Formulate the penalty term f_t^{PEN} at each time as:

$$f_t^{\text{PEN}} = \frac{1}{2} \sum_{i \in \mathcal{N}} \sum_{n \in \Omega_i^{\text{NY}}} \sum_{\alpha \in \Phi_i} |\mu_{i,n,\alpha,t}^{\text{PY}} - \mu_{i,n,\alpha,t-1}^{\text{PY}}| \quad (33)$$

- 2: Determine the coefficient ξ^{PEN} ;
 - 3: Update the objective function as $F_t^{\text{I}} = F_t + \xi^{\text{PEN}} f_t^{\text{PEN}}$;
 - 4: Formulate the new subproblem $\mathcal{P}_{2,m}^{\text{I}}(t)$ by updating F_t^{I} as the objective and dropping constraints (2) and (5);
 - 5: **for** $t \in \mathcal{T}_m$ **do**
 - 6: Solve $\mathcal{P}_{2,m}^{\text{I}}(t)$ successively using Algorithm 1;
 - 7: **end for**
 - 8: Obtain the action decisions of PSDs in \mathcal{T}_m ;
 - 9: Classify Ω^{PY} into groups $\Omega_{\text{aw}}^{\text{PY}}$ (action within limits) and $\Omega_{\text{ao}}^{\text{PY}}$ (action out of limits);
 - 10: Ensure that PSDs in $\Omega_{\text{ao}}^{\text{PY}}$ satisfy the range requirement.
- #### STEP II: Bounding
- 11: Fix the action decisions of PSDs in $\Omega_{\text{ao}}^{\text{PY}}$ based on the optimization result in **STEP I**;
 - 12: Add the above constraints to the original $\mathcal{P}_{2,m}$ and formulate the new problem $\mathcal{P}_{2,m}^{\text{II}}$ in period \mathcal{T}_m ;
 - 13: Solve $\mathcal{P}_{2,m}^{\text{II}}$ by Algorithm 1.
-

that are located in *red* nodes. Besides, two pairs of PS-SOPs are installed between different nodes. The capacity of each PS-SOP terminal is 200 kVA, and the loss coefficient λ^{S} is set as 0.02 [60]. It should be noted that the network still operates in the radial style when extra nodes are connected with PS-SOPs. Because the added virtual lines obey the operation principle of SOPs in (1) instead of the power flow in (8) [21]. Load demand curves of all the users and the net load curves with DER generation in the network are presented in Fig. 5. The proposed strategy is implemented with PYOMO [61] toolbox with Python 3.9 and solved by GUROBI [62]. All algorithms are executed on a computer with a 3.40 GHz Intel Xeon(R) CPU with 160GB of RAM. The case results can be reproduced according to the case settings provided in [63] and the proposed models as well as solution algorithms.

B. Algorithm Performance

In the objective function (6), each cost factor is chosen based on the desired priority order. In our case, the electricity price is 0.08 \$/kWh, and the cost factors are set as $c^{\text{UNB}} = 0.10, c^{\text{LOSS}} = 0.08, c^{\text{CUR}} = 0.12, c^{\text{FL}} = 0.12$. The utilized cost parameters reflect a certain priority order from DN operators, which can be applied with any more realistic costs. Besides, two coefficients ξ_1 and ξ_2 in the unbalance level function (7a) are set as 0.2 and 0.8, respectively, to balance the value magnitude. Considering the tradeoff between the balancing performance and the power supply quality, the

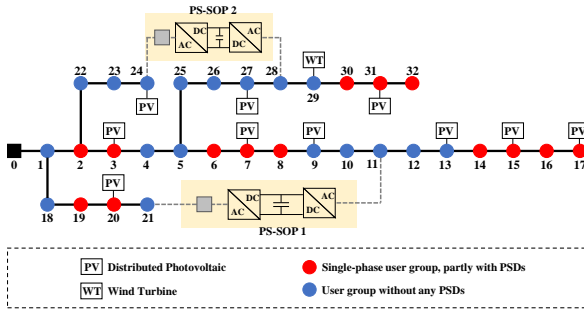


Fig. 4. Topology of the modified three-phase IEEE-33 network.

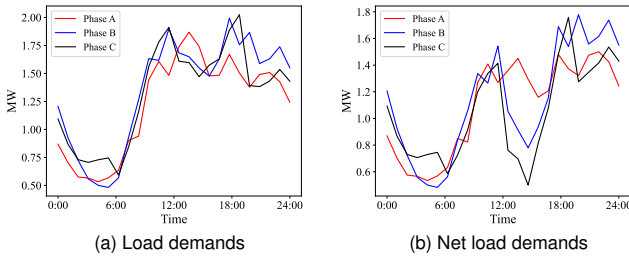


Fig. 5. Load profile and net load profile.

operation period 24h is divided into $M = 8$ phase-switching periods, and the upper limit of action times is 1 (i.e., PSDs can not be switched more than once every three hours) in our case. The installation ratio of PSDs is set as 20% (i.e., 48 users are installed with PSDs) in the network.

In the linearization process, parameters of L and M_{big} are set as 8 and 80, respectively, based on the tradeoff between approximation error and computational efficiency. In Algorithm 1, the flat start ($V = 1.0$ p.u., $[\theta^a, \theta^b, \theta^c] = [0^\circ, -120^\circ, 120^\circ]$) for each node is taken as initialization, and the thresholds $\varepsilon_1, \varepsilon_2$ are both set as 1×10^{-4} . Instead of the flat start, it is feasible to take voltage solutions of the last phase-switching period as a “warm start” for the iteration of the next period. This kind of initialization settings is beneficial to improve computational efficiency by providing an initial value around the possible optimal solution and thus reducing the iterations.

The proposed method of Algorithm 1 can automatically satisfy the feasibility condition of power flow after iteration by setting ε_2 . The feasibility of other approximations in Subsection IV-B is also ensured when compared with the original constraints. Furthermore, the convergence process of all the phase-switching periods is presented in Fig. 6a, where y -axis represents the final objective value in (6). By setting the same flat start, the optimization problems in each period converge to the optimal solution with different iterations, ranging from 4 to 16. Besides, we also notice that all the iterations tend to be relatively stable after several iterations. Because both the objective error ε_{obj} and the power solution error $\varepsilon_p, \varepsilon_q$ are set as criteria for iteration termination, the successive algorithm can not stop until both the objective accuracy and the power flow feasibility are guaranteed. Besides, the convergence process

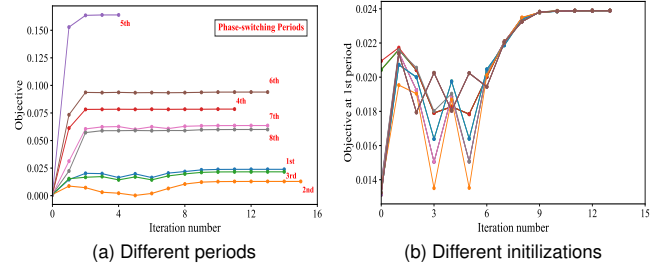


Fig. 6. Convergence under different scenarios and settings.

with different initialization settings in the first phase-switching periods is presented in Fig. 6b. It can be seen that the objective function tends to converge to the same value after several iterations, thus providing empirical evidence that the algorithm is not sensitive to initialization conditions.

C. Network Balancing Performance

Five cases are proposed to compare the different performances on network balancing of PSDs and PS-SOPs. According to whether different phase balancing devices (PSD, regular SOP, or the proposed PS-SOP) are considered, the cases include 1) “no PSD & SOP”, 2) “only PSD”, 3) “only PS-SOP”, 4) “PSD & SOP”, and 5) “PSD & PS-SOP” (*the proposed*). Besides the unbalance representation in the constraint (14), four metrics are then utilized to evaluate the unbalance mitigation performance in the objective function, which is also helpful to ensure the effectiveness of the linearization process for (14). The definitions of metrics are formulated as follows.

$$\text{VUB}_1 = \sum_{i \in \mathcal{N}} \left| \frac{\tilde{V}_i^{\text{NEG}}}{\tilde{V}_i^{\text{POS}}} \right|, \quad \text{VUB}_2 = \sum_{i \in \mathcal{N}} \left| \frac{\tilde{V}_i^{\text{ZER}}}{\tilde{V}_i^{\text{POS}}} \right| \quad (34a)$$

$$\text{IUB}_1 = \left| \frac{\tilde{I}_0^{\text{NEG}}}{\tilde{I}_0^{\text{POS}}} \right|, \quad \text{IUB}_2 = \left| \frac{\tilde{I}_0^{\text{ZER}}}{\tilde{I}_0^{\text{POS}}} \right| \quad (34b)$$

where VUB_1 and VUB_2 are used to evaluate both the magnitude and phase unbalance of voltages; similarly, after calculating the phase current injection in the root node and the corresponding sequence current components, IUB_1 and IUB_2 are formulated to evaluate the current unbalance.

After formulating and solving \mathcal{P}_2 based on Algorithm 1, results of the unbalance metrics of all cases are given in Fig. 7. The trends of metrics varying in different periods are similar among all the cases, and the proposed method can achieve the best balancing performance at most phase-switching periods. In Figs. 7a-7b, the three-phase voltage reaches the highest unbalance level at about 12:00, due to the unbalanced PV generation and load behaviors. Compared with “no PSD & SOP”, the proposed method reduces VUB_1 from 0.25 to 0.07. Besides, for the current unbalance metrics in Figs. 7c-7d, the proposed method can maintain a relatively low level at most periods (e.g., $[0, 0.1]$ of IUB_1). It is noticed that metrics IUB_1 and IUB_2 of the proposed method increase at period 13:00-14:00, which is the trade-off to mitigate the voltage unbalance level. Therefore, both voltage and current unbalance conditions are mitigated into the comprehensively lowest level by the

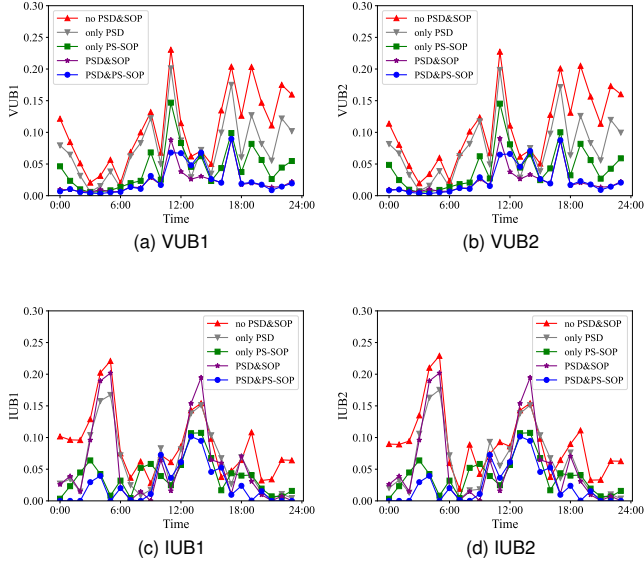


Fig. 7. Voltage and current unbalance metrics.

proposed method in the operation period. Besides, it can be seen that the varying trend of VUB_1/IUB_1 is similar with VUB_2/IUB_2 , which show that the proposed representation of unbalance levels in the objective function can perform an approximately equal influence for both the negative and zero sequence voltage unbalance.

Comparisons of other cases show that PSDs and PS-SOPs can perform different functions in network balancing. For voltage balancing, using only PSDs or PS-SOPs can only lightly reduce the unbalance level (e.g., from 0.25 to 0.15-0.20 of VUB_1 at 12:00), but coordinating PSDs with either regular SOPs or PS-SOPs can reduce it to about 0.08. It can be seen that PSDs perform better for node voltage balancing because they are distributed among nodes and more suitable for local voltage balancing. For current balancing, PS-SOPs can achieve better mitigation performance compared with SOPs or PSDs, and no obvious improvements are seen in the unbalance mitigation when coordinated with PSDs than not. Therefore, the phase-switching function of the proposed PS-SOP performs important functions on the network current balancing because it can transfer currents among phases and nodes directly.

Four parts in the objective function including the unbalance level, network loss, renewable curtailment, and load alteration of the five cases are presented in Fig. 8. It can be seen that the proposed method can be optimized with the minimum objective value. Because of the flexible phase switching and the cross-node power transfer functions, the proposed method reduces the unbalance level and the renewable curtailment obviously, especially during the 4th-6th periods. Besides, although the implementation of SOPs causes an extra loss in inverters during the operation process, the proposed method can maintain the whole loss at a similar level to the original case, which verifies that the proposed method can mitigate network unbalance without increasing network loss.

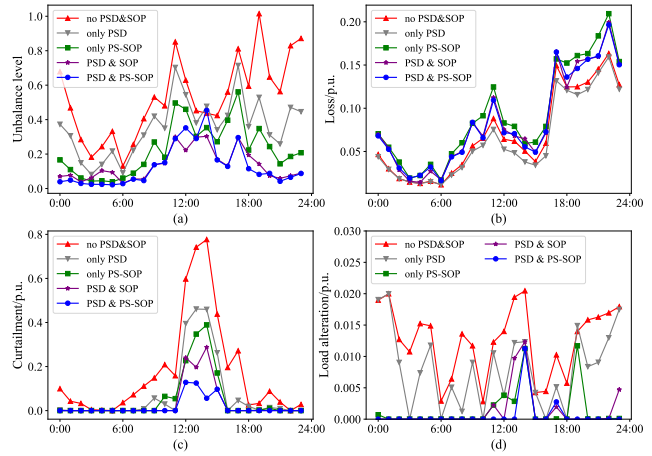


Fig. 8. Objective terms (without cost factors): (a) unbalance level, (b) network loss, (c) renewable curtailment, (d) load alteration.

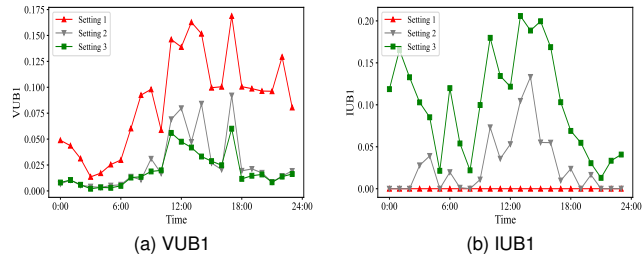


Fig. 9. Voltage and current unbalance metrics with different weight settings.

D. Sensitivity Analysis

1) *Parameter*: While keeping other parameters the same with the above case, we first demonstrate the sensitivity of the objective weight ξ_1, ξ_2 on power/voltage balance levels. Three settings are performed including **Setting 1**: $\xi_1 = 1, \xi_2 = 0$, **Setting 2 (the proposed)**: $\xi_1 = 0.2, \xi_2 = 0.8$, and **Setting 3**: $\xi_1 = 0, \xi_2 = 1$. The unbalance levels are presented in Fig. 9 with VUB_1, IUB_1 for evaluation. It can be seen that different weight settings directly influence the balancing performance, where ξ_1 and ξ_2 represent the importance of current and voltage balancing, respectively.

In the proposed coordination method of PSDs and PS-SOPs, key parameters including the installation ratio of PSDs and the capacities of PS-SOPs contribute to different balancing performances. The objective values are implemented to explore the influences of various combinations of PSD installation ratios and SOP capacities.

The results are given in Fig. 10, where solid and dashed lines represent the PS-SOPs and regular SOPs that are utilized in DNs, respectively. It can be seen that objective values keep declining but the decline rates become slower with higher PSD installation ratios or larger SOP capacities. In the proposed method, coordination settings of the capacity range of 100-200 kVA and the installation ratio range of 0.05-0.15 have contributed to higher decline rates than other combinations. Changing trends of objective values become stable when

TABLE II
PERFORMANCE AND ANNUAL COST COMPARISON ON IMPLEMENTATIONS

Implementation	avg. VUB1	avg. VUB2	avg. IUB1	avg. IUB2	Annual cost of operation (\$)	Annual cost of devices (\$)	Total cost (\$)
Initial case	0.1103	0.1083	0.0871	0.0901	243,403.43	0	243,403.43
PV [14]	0.1037	0.1040	0.0836	0.0823	123,989.94	566.67	124,556.61
Capacitor Bank [10]	0.0576	0.0578	0.0536	0.0536	151,903.85	1,145.01	153,048.86
Only PSD	0.0794	0.0794	0.0613	0.0633	130,092.35	4,056.71	134,149.06
Only PS-SOP	0.0504	0.0500	0.0434	0.0434	121,230.66	27,631.97	148,862.63
PSD&PS-SOP	0.0264	0.0260	0.0275	0.0275	77,523.13	31,688.68	109,211.81

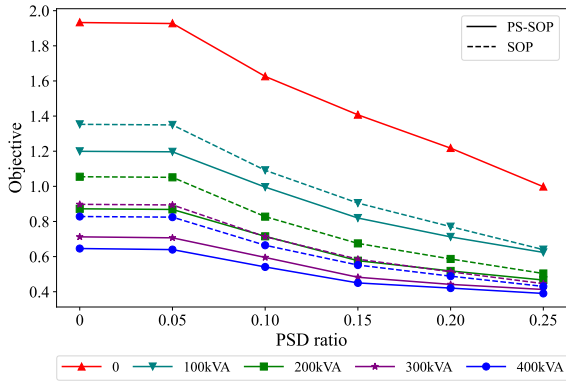


Fig. 10. Objective values with different parameters.

continuing to increase the PSD installation ratio to more than 0.20 or PS-SOP capacity to more than 200 kVA, which can be potentially uneconomic investment choices. Besides, with smaller capacities, PS-SOPs can achieve a similar balancing performance compared with SOPs. For example, when replacing 300 kVA SOPs with 200 kVA PS-SOPs, the changing trend of objective values keeps similar when the PSD installation ratio increases from 0 to 0.25. It can be seen that the phase-switching function can help reduce the extra investment in SOP capacities.

2) *Cost*: Furthermore, to analyze the economical feasibility of the proposed balancing strategy, we compare it with the commonly adopted means in the same case, including the three-phase PVs [14] and capacitor banks [10]. The balancing performance is evaluated by the average values of four metrics VUB_1 - IUB_2 . The detailed annual cost calculation method and corresponding parameters are presented in Appendix-C. As a common type of DERs, the additional investment cost of three-phase PVs is not considered. For PS-SOPs, the cost of the power electronics (e.g., the inverters connected with three-phase nodes) will be the dominant cost, and we take the typical value in [60] for the cost parameter reference. The result of each strategy is given in Table II.

In terms of the network balancing performance, the proposed method can achieve the lowest unbalance level compared with other commonly used methods. Besides, although the annual cost of the applied equipment is relatively high, the total cost is lower than others because of the less cost of distribution network operation. Compared with the single means, the proposed two-level coordination strategy can perform bet-

ter in both network balancing and economic operation. Thus, an “economy of scale” can be achieved by the complementary advantages of PS-SOPs and PSDs.

3) *Computational efficiency*: Furthermore, the computation becomes more difficult with higher installation ratios of PSDs in the network, so we verify the computational efficiency performance of the proposed Algorithm 2 under different PSD installation ratios. The ratio keeps the same in all the nodes with PSDs and varies from 0.2 to 0.4. Three representative phase-switching periods (0:00-3:00, 18:00-21:00, and 21:00-24:00) are determined by the actual computational time with different PSD ratios. Comparison results on computational time and solution accuracy in these periods are given in Table III, where the key parameter ξ^{PEN} is determined in advance based on Remark 1 in Subsection IV-C. The relative error is calculated as $ERR = \frac{|F^{II} - F^*|}{F^*} \times 100\%$. From the result of the original case, the computational time increases with a larger number of installed PSDs, and its growth rate varies with load scenarios in different phase-switching periods. The proposed Algorithm 2 can largely reduce the computation time with an acceptable loss of accuracy. When the PSD installation ratio increases above 0.3, the computation time of Algorithm 1 is around or over 1000s at each period. However, the proposed method can still solve the problem within 300s in all cases and within 200s in most cases. Therefore, the computational efficiency of the proposed algorithm is acceptable in the day-ahead dispatch task. As for the accuracy of the proposed algorithm, Step I in Algorithm 2 can optimize with a preliminarily lower objective value than Algorithm 1 because of the relaxation. The relative errors after bounding in Step II in all cases are lower than 10%, which shows that the proposed algorithm can largely improve computational efficiencies with acceptable loss of accuracy.

E. Scalability Tests

To demonstrate the computational complexity of the proposed algorithm on larger networks, we further adopt a three-phase IEEE 123-Bus network [64] and a standard three-phase 240-bus distribution network in Midwest U.S. [65] for more case studies. The load levels of three phase lines during 24h are presented in Table IV. More details on the parameter settings are presented in the supplementary files [63]. Three phase-switching periods corresponding to IEEE 33-bus network case are evaluated. The computational time as well as the objective values are presented in Tables V and VI, respectively.

From the result of each network, it can be seen that: 1) with higher PSD ratios, the computational time in the original

TABLE III
COMPUTATIONAL EFFICIENCY WITH THE PROPOSED SOLUTION ALGORITHM

PSD ratio (number)	Operation period	Computation time (s)		Objective			Coefficient ξ^{PEN}	
		Alg.1	Alg.2	F^* of Alg.1	F after relaxation	F^{II} of Alg.2		ERR (%)
0.20(48)	0:00-3:00	183.92	110.86	0.01995	0.01946	0.02102	5.36	0.05
	18:00-21:00	99.90	97.26	0.05327	0.05215	0.05330	0.06	0.02
	21:00-24:00	104.88	111.53	0.04813	0.04793	0.04956	2.97	0.005
0.25(63)	0:00-3:00	638.33	173.47	0.01740	0.01674	0.01833	5.34	0.01
	18:00-21:00	757.54	121.19	0.04832	0.04513	0.05211	7.84	0.01
	21:00-24:00	1097.44	139.85	0.04457	0.04270	0.04772	7.07	0.005
0.30(73)	0:00-3:00	905.54	148.65	0.01584	0.01538	0.01708	7.83	0.05
	18:00-21:00	1193.75	152.55	0.04290	0.04280	0.04482	4.48	0.01
	21:00-24:00	1429.35	141.28	0.04117	0.04068	0.04551	10.54	0.05
0.35(79)	0:00-3:00	2280.01	252.71	0.01475	0.01404	0.01549	5.02	0.01
	18:00-21:00	2459.12	138.22	0.04000	0.03985	0.04096	2.40	0.01
	21:00-24:00	3838.34	209.16	0.04033	0.03996	0.04284	6.22	0.03
0.40(94)	0:00-3:00	2682.02	191.21	0.01444	0.01424	0.01572	8.86	0.02
	18:00-21:00	4258.98	152.60	0.03771	0.03768	0.04018	6.55	0.01
	21:00-24:00	> 5h	284.23	/	0.03923	0.04385	/	0.02

case has a similar increasing trend with IEEE 33-bus network; 2) the proposed algorithm can reduce the computational time effectively, especially under higher PSD ratios, and the time varying trend is slightly influenced by the increased ratio of installed PSDs (e.g., 200-400s in IEEE 123-bus case and 400-800s in U.S. 240-bus case). From the comparison results in different networks, some new features can be found: 1) the computational time of both the original case and the proposed algorithm basically increase with more complex network topologies and higher load levels, however, the growth rate in the original case is more obviously influenced by the PSD installation ratios; 2) the computational time is also relevant with the objective performance. For example, when comparing the 0:00-3:00 period with 113 installed PSDs, the computational time is around 3200s in IEEE 123-bus network, and about 700s in U.S. 240-bus network. It can be seen that the IEEE 123-bus network spends more time in optimization but the objective improvement is not obvious compared with PSD ratio=0.35. It is mainly because the optimization process will spend more time determining the optimal actions of specific PSDs, especially which make fewer contributions to objective improvement.

Therefore, when applied in larger networks, we can conclude that the computational complexity is more dependent on the number of controllable devices (i.e., the number of integer variables in the model) than the network topology complexity. Our proposed algorithm can efficiently ease the computational burden brought by massive integer variables in the original model. Furthermore, it is possible to extend the proposed method for larger networks (e.g., IEEE 8700-bus network [66]), with some accelerated OPF solving algorithms in some related research [67]–[69].

VI. CONCLUSIONS AND FUTURE WORKS

We formulate a two-level coordination model of PSDs and PS-SOPs for network balancing. The proposed method is validated to achieve the best performances on both voltage

TABLE IV
LOAD LEVELS (MW)

	Phase A	Phase B	Phase C
IEEE 123-bus	4.99	5.00	4.14
U.S. 240-bus	10.10	9.78	8.24

TABLE V
COMPUTATIONAL EFFICIENCY IN IEEE 123-BUS SYSTEM

PSD ratio (number)	Operation period	Computation time (s)		Objective		
		Alg.1	Alg.2	F^* of Alg.1	F^{II} of Alg.2	ERR (%)
0.20(68)	0:00-3:00	568.71	455.34	0.02929	0.03000	2.42
	18:00-21:00	154.92	130.55	0.06387	0.06393	0.09
	21:00-24:00	146.97	126.97	0.05262	0.05322	1.14
0.25(89)	0:00-3:00	842.06	474.41	0.02732	0.02882	5.49
	18:00-21:00	273.18	139.13	0.06029	0.06377	5.77
	21:00-24:00	174.36	127.95	0.04996	0.05203	4.14
0.30(105)	0:00-3:00	1276.38	473.36	0.02658	0.02774	4.36
	18:00-21:00	280.94	134.76	0.05921	0.06150	3.87
	21:00-24:00	526.38	257.28	0.04774	0.04939	3.46
0.35(113)	0:00-3:00	2149.37	374.24	0.02647	0.02735	3.32
	18:00-21:00	350.45	171.96	0.05867	0.06035	2.86
	21:00-24:00	540.93	280.13	0.04742	0.04954	4.47
0.40(135)	0:00-3:00	3222.54	340.10	0.02612	0.02712	3.67
	18:00-21:00	1018.54	138.87	0.05502	0.05761	4.71
	21:00-24:00	787.21	157.72	0.04580	0.04661	1.76

and current balancing. Specifically, the PSDs contribute more to local voltage balancing because they are distributed locally within network nodes. On this basis, the proposed PS-SOPs can transfer active power among different phases and nodes for the redistribution of three-phase currents. Besides, we propose a solution framework with two algorithms, which can ensure optimal solutions and accelerate the computation simultaneously. The proposed algorithms extend the application of the coordination model for different levels of PSD integration.

For the proposed coordination balancing strategy, this work focuses on the technical superiority analysis to verify the network balancing performance. The future research is concluded with the following points: 1) perform more discussions on the cost-benefit analysis to evaluate the operation benefits with

TABLE VI
COMPUTATIONAL EFFICIENCY IN U.S. 240-BUS SYSTEM

PSD ratio (number)	Operation period	Computation time (s)		Objective		
		Alg.1	Alg.2	F^* of Alg.1	F^H of Alg.2	ERR (%)
0.20(114)	0:00-3:00	703.93	509.58	0.13676	0.13698	0.16
	18:00-21:00	471.72	391.53	0.52589	0.52757	0.32
	21:00-24:00	459.85	424.60	0.46669	0.47105	0.93
0.25(146)	0:00-3:00	3755.48	791.50	0.12306	0.12620	2.55
	18:00-21:00	501.83	431.44	0.45510	0.45571	0.13
	21:00-24:00	506.39	432.37	0.37597	0.38206	1.62
0.30(170)	0:00-3:00	4304.76	752.11	0.12199	0.12432	1.91
	18:00-21:00	536.25	431.53	0.44449	0.44500	0.11
	21:00-24:00	610.81	444.49	0.35794	0.36273	1.34
0.35(185)	0:00-3:00	> 5h	902.25	/	0.11401	/
	18:00-21:00	545.53	436.06	0.39615	0.39737	0.31
	21:00-24:00	890.66	448.16	0.32091	0.33065	3.04
0.40(220)	0:00-3:00	> 5h	892.84	/	0.10837	/
	18:00-21:00	773.34	449.82	0.37390	0.37743	0.94
	21:00-24:00	2196.58	453.07	0.30170	0.31349	3.91

regard to the investment costs; 2) consider the probabilistic characteristics of renewable generation in the decision-making process; 3) optimize the parameters corresponding to the phase-switching periods for better balancing solutions; 4) explore and extend the phase-balancing function of PSDs for three-phase users or single-phase PVs.

APPENDIX

A. Current Unbalance Influence on Operation Cost

1) *Cost on phase line loss*: We take a three-phase two-bus system as an example, where one bus is for power supply and another one is the sum of load demands. Supposed that the whole phase current is a constant $|I^S|$ and the phase resistances are the same $R^{aa} = R^{bb} = R^{cc} = R$, the network loss can be represented as

$$|I^a| + |I^b| + |I^c| = |I^S| \quad (35a)$$

$$\begin{aligned} Loss &= |I^a|^2 R^{aa} + |I^b|^2 R^{bb} + |I^c|^2 R^{cc} \\ &= (|I^a|^2 + |I^b|^2 + |I^c|^2)R \end{aligned} \quad (35b)$$

Based on Cauchy's Inequality theory, we have the following relationship.

$$\begin{aligned} |I^a|^2 + |I^b|^2 + |I^c|^2 &= \frac{(1+1+1)(|I^a|^2 + |I^b|^2 + |I^c|^2)}{3} \\ &\geq \frac{(|I^a| + |I^b| + |I^c|)^2}{3} = \frac{|I^S|^2}{3} \end{aligned} \quad (36)$$

where the equation has the minimum value when $|I^a| = |I^b| = |I^c|$. Thus, it can be derived that the balanced current magnitude will result in the minimum phase line loss.

2) *Cost on neutral line loss*: In the three-phase-four-wire distribution network, the relationship between node voltages and line currents is

$$\begin{aligned} \begin{bmatrix} \tilde{V}_i^a \\ \tilde{V}_j^a \\ \tilde{V}_i^b \\ \tilde{V}_j^b \\ \tilde{V}_i^c \\ \tilde{V}_j^c \\ \tilde{V}_i^n \\ \tilde{V}_j^n \end{bmatrix} - \begin{bmatrix} \tilde{V}_j^a \\ \tilde{V}_i^a \\ \tilde{V}_j^b \\ \tilde{V}_i^b \\ \tilde{V}_j^c \\ \tilde{V}_i^c \\ \tilde{V}_j^n \\ \tilde{V}_i^n \end{bmatrix} &= \begin{bmatrix} z_{ij}^{aa} & z_{ij}^{ab} & z_{ij}^{ac} & z_{ij}^{an} \\ z_{ij}^{ba} & z_{ij}^{bb} & z_{ij}^{bc} & z_{ij}^{bn} \\ z_{ij}^{ca} & z_{ij}^{cb} & z_{ij}^{cc} & z_{ij}^{cn} \\ z_{ij}^{na} & z_{ij}^{nb} & z_{ij}^{nc} & z_{ij}^{nn} \end{bmatrix} \cdot \begin{bmatrix} \tilde{I}_{ij}^a \\ \tilde{I}_{ij}^b \\ \tilde{I}_{ij}^c \\ \tilde{I}_{ij}^n \end{bmatrix} \\ \Leftrightarrow \begin{bmatrix} \tilde{V}_i^{abc} \\ \tilde{V}_j^{abc} \\ \tilde{V}_i^n \\ \tilde{V}_j^n \end{bmatrix} - \begin{bmatrix} \tilde{V}_j^{abc} \\ \tilde{V}_i^{abc} \\ \tilde{V}_j^n \\ \tilde{V}_i^n \end{bmatrix} &= \begin{bmatrix} (\mathbf{z}_{ij}^{\alpha\beta})_{3 \times 3} & (\mathbf{z}_{ij}^{\alpha n})_{3 \times 1} \\ (\mathbf{z}_{ij}^{n\beta})_{1 \times 3} & (\mathbf{z}_{ij}^{nn})_{1 \times 1} \end{bmatrix} \cdot \begin{bmatrix} \tilde{I}_{ij}^{abc} \\ \tilde{I}_{ij}^n \end{bmatrix} \end{aligned} \quad (37)$$

It is assumed that this network has a multi-grounded neutral, thus the neutral voltage is equal to zero. The unbalanced phase current will generate the zero sequence current flowing in the neutral lines, and thus increase the neutral line loss due to the mutual impedance. To incorporate the extra loss into the three-phase model, we use the Kron reduction principle and reduce the 4×4 impedance matrix as 3×3 , so the neutral line loss is included in the phase line loss functions.

$$\begin{aligned} \begin{cases} \tilde{V}_i^{abc} - \tilde{V}_j^{abc} = \mathbf{z}_{ij}^{\alpha\beta} \cdot \tilde{I}_{ij}^{abc} + \mathbf{z}_{ij}^{\alpha n} \cdot \tilde{I}_{ij}^n \\ 0 = \mathbf{z}_{ij}^{n\beta} \cdot \tilde{I}_{ij}^{abc} + \mathbf{z}_{ij}^{nn} \tilde{I}_{ij}^n \end{cases} \\ \Leftrightarrow \begin{cases} \tilde{I}_{ij}^n = -(\mathbf{z}_{ij}^{nn})^{-1} \mathbf{z}_{ij}^{n\beta} \cdot \tilde{I}_{ij}^{abc} \\ \tilde{V}_i^{abc} - \tilde{V}_j^{abc} = (\mathbf{z}_{ij}^{\alpha\beta} - \mathbf{z}_{ij}^{\alpha n} (\mathbf{z}_{ij}^{nn})^{-1} \mathbf{z}_{ij}^{n\beta}) \cdot \tilde{I}_{ij}^{abc} \end{cases} \end{aligned} \quad (38)$$

Then we can obtain the phase impedance matrix on the line ij as $(\mathbf{z}_{ij})_{3 \times 3} = \mathbf{z}_{ij}^{\alpha\beta} - \mathbf{z}_{ij}^{\alpha n} (\mathbf{z}_{ij}^{nn})^{-1} \mathbf{z}_{ij}^{n\beta}$, where the neutral line loss is also included.

B. Voltage Unbalance Representation

To verify the effectiveness of the proposed voltage unbalance representation method in the objective function, we compare it with the commonly used sequence voltage components. We first set the varying ranges of voltage magnitude and angle as ± 0.01 p.u. and $\pm 3^\circ$, respectively, and then we generate 729 samples of three-phase voltage randomly. After calculation, the relationship is represented in Fig. 11, where the x axis is $(f_V^{\text{UNB}} + f_\theta^{\text{UNB}})$, and the y axis is the magnitude of negative sequence voltage in (14c) and zero sequence voltage in (14d), respectively. There is a roughly positive correlation between the proposed unbalance representation and the commonly used ones. Therefore, the proposed method can represent the voltage unbalance level effectively, i.e., minimization of $f_V^{\text{UNB}} + f_\theta^{\text{UNB}}$ can reduce the unbalance level directly.

C. Annual Cost Calculation

The annual cost C_{total} mainly includes the equivalent annual capital cost C_{install} , the fixed device operation cost C_{ope} , and

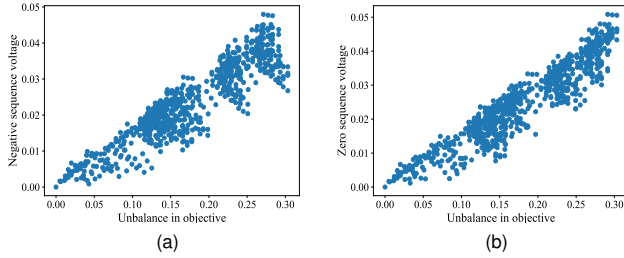


Fig. 11. Relationship between the unbalance level in the objective and the magnitude of: (a) negative sequence voltage; (b) zero sequence voltage.

TABLE VII
 COST-RELATED PARAMETERS OF EQUIPMENT

Equipment	Number	Lifetime (year)	Capital cost (\$)	Cost coefficient
PV inverter	10	10	25.0/kW	0.02
Capacitor bank	6	10	30.0/piece	0.01
PSD	48	10	500.0/piece	0.02
SOP	2	20	308.8/kVA	0.01

the cost in distribution network operation from the objectives C_{obj} . The detailed cost calculation method is presented as

$$C_{total} = C_{install} + C_{ope} + C_{obj} \quad (39a)$$

$$C_{install} = \frac{d(1+d)^y}{(1+d)^y - 1} \sum_{i=1}^{N_{unit}} c_{unit,i} S_{unit,i} \quad (39b)$$

$$C_{ope} = \eta_{ope} \sum_{i=1}^{N_{unit}} c_{unit,i} S_{unit,i} \quad (39c)$$

$$C_{obj} = 365 \cdot \sum_{t=1}^{\mathcal{T}} (C_t^{LOSS} + C_t^{CUR} + C_t^{FL}), \quad \mathcal{T} = 24h \quad (39d)$$

where d , y , N_{unit} , c_{unit} , S_{unit} , and η_{ope} are the discount rate, the lifetime, the installation number, the capital cost, the installation capacity, and the coefficient of operation cost, respectively. d is set as 0.08, and other key parameters (installation number N_{unit} , lifetime y , capital cost c_{unit} , and coefficient of operation cost η_{ope}) are given in Table VII.

REFERENCES

- [1] K. Ma, L. Fang, and W. Kong, "Review of distribution network phase unbalance: Scale, causes, consequences, solutions, and future research directions," *CSEE Journal of Power and Energy Systems*, vol. 6, no. 3, pp. 479–488, 2020.
- [2] K. Ma, R. Li, and F. Li, "Utility-scale estimation of additional reinforcement cost from three-phase imbalance considering thermal constraints," *IEEE Transactions on Power Systems*, vol. 32, no. 5, pp. 3912–3923, 2016.
- [3] D. Q. Hung and Y. Mishra, "Impacts of single-phase pv injection on voltage quality in 3-phase 4-wire distribution systems," in *2018 IEEE Power & Energy Society General Meeting (PESGM)*. IEEE, 2018, pp. 1–5.
- [4] S. Liu, X. Cui, Z. Lin, Z. Lian, Z. Lin, F. Wen, Y. Ding, Q. Wang, L. Yang, R. Jin, and H. Qiu, "Practical method for mitigating three-phase unbalance based on data-driven user phase identification," *IEEE Transactions on Power Systems*, vol. 35, no. 2, pp. 1653–1656, 2020.
- [5] O. Pereira, J. Quirós-Tortós, and G. Valverde, "Phase rebalancing of distribution circuits dominated by single-phase loads," *IEEE Transactions on Power Systems*, vol. 36, no. 6, pp. 5333–5344, 2021.
- [6] O. Homaei, A. Najafi, M. Dehghanian, M. Attar, and H. Falaghi, "A practical approach for distribution network load balancing by optimal re-phasing of single phase customers using discrete genetic algorithm," *International Transactions on Electrical Energy Systems*, vol. 29, no. 5, p. e2834, 2019.
- [7] X. Zeng, H. Zhai, M. Wang, M. Yang, and M. Wang, "A system optimization method for mitigating three-phase imbalance in distribution network," *International Journal of Electrical Power & Energy Systems*, vol. 113, pp. 618–633, 2019.
- [8] B. Liu, K. Meng, Z. Y. Dong, P. K. Wong, and T. Ting, "Unbalance mitigation via phase-switching device and static var compensator in low-voltage distribution network," *IEEE Transactions on Power Systems*, vol. 35, no. 6, pp. 4856–4869, 2020.
- [9] A. Nakadomari, R. Shigenobu, and T. Senjyu, "Optimal control and placement of step voltage regulator for voltage unbalance improvement and loss minimization in distribution system," in *2020 IEEE REGION 10 CONFERENCE (TENCON)*, 2020, pp. 1013–1018.
- [10] M. Chamana and B. H. Chowdhury, "Optimal voltage regulation of distribution networks with cascaded voltage regulators in the presence of high PV penetration," *IEEE Transactions on Sustainable Energy*, vol. 9, no. 3, pp. 1427–1436, 2018.
- [11] J. Wang, N. Zhou, Y. Ran, and Q. Wang, "Optimal operation of active distribution network involving the unbalance and harmonic compensation of converter," *IEEE Transactions on Smart Grid*, vol. 10, no. 5, pp. 5360–5373, 2019.
- [12] M. Yao, I. A. Hiskens, and J. L. Mathieu, "Mitigating voltage unbalance using distributed solar photovoltaic inverters," *IEEE Transactions on Power Systems*, vol. 36, no. 3, pp. 2642–2651, 2021.
- [13] J. Li, Z. Hai, Z. Shuai, L. Zhu, X. Xu, C. Zhang, and J. Zhao, "Coordinated current and voltage unbalance mitigation in networked microgrids with aggregated pv systems," *IEEE Transactions on Power Systems*, 2022.
- [14] A. Gastalver-Rubio, E. Romero-Ramos, and J. M. Maza-Ortega, "Improving the performance of low voltage networks by an optimized unbalance operation of three-phase distributed generators," *IEEE Access*, vol. 7, pp. 177 504–177 516, 2019.
- [15] R. Gupta, S. Fahmy, and M. Paolone, "Coordinated day-ahead dispatch of multiple power distribution grids hosting stochastic resources: An admm-based framework," *Electric Power Systems Research*, vol. 212, p. 108555, 2022.
- [16] W. Cao, J. Wu, N. Jenkins, C. Wang, and T. Green, "Benefits analysis of soft open points for electrical distribution network operation," *Applied Energy*, vol. 165, pp. 36–47, 2016.
- [17] Q. Qi, J. Wu, and C. Long, "Multi-objective operation optimization of an electrical distribution network with soft open point," *Applied Energy*, vol. 208, pp. 734–744, 2017.
- [18] J. Wang, N. Zhou, C. Chung, and Q. Wang, "Coordinated planning of converter-based DG units and soft open points incorporating active management in unbalanced distribution networks," *IEEE Transactions on Sustainable Energy*, vol. 11, no. 3, pp. 2015–2027, 2019.
- [19] P. Li, H. Ji, C. Wang, J. Zhao, G. Song, F. Ding, and J. Wu, "Optimal operation of soft open points in active distribution networks under three-phase unbalanced conditions," *IEEE Transactions on Smart Grid*, vol. 10, no. 1, pp. 380–391, 2019.
- [20] F. Sun, J. Ma, M. Yu, and W. Wei, "Optimized two-time scale robust dispatching method for the multi-terminal soft open point in unbalanced active distribution networks," *IEEE Transactions on Sustainable Energy*, vol. 12, no. 1, pp. 587–598, 2020.
- [21] M. Deakin, P. C. Taylor, J. Bialek, and W. Ming, "Design and operation of hybrid multi-terminal soft open points using feeder selector switches for flexible distribution system interconnection," *Electric Power Systems Research*, vol. 212, p. 108516, 2022.
- [22] C. Lou, J. Yang, T. Li, and E. Vega-Fuentes, "New phase-changing soft open point and impacts on optimising unbalanced power distribution networks," *IET Generation, Transmission & Distribution*, vol. 14, no. 23, pp. 5685–5696, 2020.
- [23] C. Lou, J. Yang, E. Vega-Fuentes, N. K. Meena, and L. Min, "Multi-terminal phase-changing soft open point sdg modeling for imbalance mitigation in active distribution networks," *International Journal of Electrical Power & Energy Systems*, vol. 142, p. 108228, 2022.
- [24] F. Shahnia, P. J. Wolfs, and A. Ghosh, "Voltage unbalance reduction in low voltage feeders by dynamic switching of residential customers among three phases," *IEEE Transactions on Smart Grid*, vol. 5, no. 3, pp. 1318–1327, 2014.
- [25] B. Liu, K. Meng, Z. Y. Dong, P. K. C. Wong, and X. Li, "Load balancing in low-voltage distribution network via phase reconfiguration:

- An efficient sensitivity-based approach," *IEEE Transactions on Power Delivery*, vol. 36, no. 4, pp. 2174–2185, 2021.
- [26] Y.-J. Kim, "Development and analysis of a sensitivity matrix of a three-phase voltage unbalance factor," *IEEE Transactions on Power Systems*, vol. 33, no. 3, pp. 3192–3195, 2018.
- [27] A. Kharrazi and V. Sreeram, "Mitigation of voltage unbalance in distribution feeders using phase switching devices: A decentralized control approach based on local measurements," *IEEE Transactions on Power Delivery*, vol. 37, no. 4, pp. 2875–2885, 2022.
- [28] B. Liu, F. Geth, N. Mahdavi, and J. Zhong, "Load balancing in low-voltage distribution networks via optimizing residential phase connections," in *2021 IEEE PES Innovative Smart Grid Technologies - Asia (ISGT Asia)*, 2021, pp. 1–5.
- [29] S. Soltani, M. Rashidinejad, and A. Abdollahi, "Dynamic phase balancing in the smart distribution networks," *International Journal of Electrical Power & Energy Systems*, vol. 93, pp. 374–383, 2017.
- [30] S. Liu, Z. Lin, J. Li, F. Wen, Y. Ding, Q. Wang, F. Lu, and L. Yang, "Bi-level optimal placement model of phase switch devices for mitigating three-phase unbalance in low-voltage areas," *IEEE Transactions on Power Systems*, vol. 37, no. 4, pp. 3149–3152, 2022.
- [31] I. I. Avramidis, F. Capitanescu, and G. Deconinck, "A comprehensive multi-period optimal power flow framework for smart LV networks," *IEEE Transactions on Power Systems*, vol. 36, no. 4, pp. 3029–3041, 2021.
- [32] S. Karagiannopoulos, P. Aristidou, and G. Hug, "A centralised control method for tackling unbalances in active distribution grids," in *2018 Power Systems Computation Conference (PSCC)*. IEEE, 2018, pp. 1–7.
- [33] L. R. de Araujo, D. R. R. Penido, S. Carneiro, and J. L. R. Pereira, "A study of neutral conductors and grounding impacts on the load-flow solutions of unbalanced distribution systems," *IEEE Transactions on Power Systems*, vol. 31, no. 5, pp. 3684–3692, 2016.
- [34] N. Nazir, P. Racherla, and M. Almassalkhi, "Optimal multi-period dispatch of distributed energy resources in unbalanced distribution feeders," *IEEE Transactions on Power Systems*, vol. 35, no. 4, pp. 2683–2692, 2020.
- [35] X. Jiang, Y. Zhou, W. Ming, P. Yang, and J. Wu, "An overview of soft open points in electricity distribution networks," *IEEE Transactions on Smart Grid*, 2022.
- [36] L. Ma, L. Wang, and Z. Liu, "Soft open points-assisted resilience enhancement of power distribution networks against cyber risks," *IEEE Transactions on Power Systems*, 2022.
- [37] Jemena: DER Hosting Capacity Project Interim Knowledge Sharing Report, [Online], <https://arena.gov.au/knowledge-bank/jemena-der-hosting-capacity-project-interim-knowledge-sharing-report/>.
- [38] AusNet: Creating solar friendly neighbourhoods, [Online], <https://www.ausnetservices.com.au/projects-and-innovation/enabling-solar-and-battery-future/#CreatingSolarFriendlyNeighbourhoods>.
- [39] K. Ma, R. Li, and F. Li, "Quantification of additional asset reinforcement cost from 3-phase imbalance," *IEEE Transactions on Power Systems*, vol. 31, no. 4, pp. 2885–2891, 2015.
- [40] K. Girigoudar, M. Yao, J. L. Mathieu, and L. A. Roald, "Integration of centralized and distributed methods to mitigate voltage unbalance using solar inverters," *IEEE Transactions on Smart Grid*, 2022.
- [41] W. Kersting, "The computation of neutral and dirt currents and power losses," in *IEEE PES Power Systems Conference and Exposition, 2004*. IEEE, 2004, pp. 213–218.
- [42] E. Standard, "50160," *Voltage characteristics of public distribution systems*, vol. 18, 2010.
- [43] D. Gebbran, S. Mhanna, A. C. Chapman, and G. Verbić, "Multiperiod DER coordination using ADMM-based three-block distributed AC optimal power flow considering inverter volt-var control," *IEEE Transactions on Smart Grid*, pp. 1–1, 2022.
- [44] M. U. Hashmi, D. Deka, A. Bušić, and D. Van Hertem, "Can locational disparity of prosumer energy optimization due to inverter rules be limited?" *IEEE Transactions on Power Systems*, pp. 1–15, 2022.
- [45] Q. Jia, Y. Li, Z. Yan, and S. Chen, "Reactive power market design for distribution networks with high photovoltaic penetration," *IEEE Transactions on Smart Grid*, 2022.
- [46] Y. Wang, N. Zhang, H. Li, J. Yang, and C. Kang, "Linear three-phase power flow for unbalanced active distribution networks with PV nodes," *CSEE Journal of Power and Energy Systems*, vol. 3, no. 3, pp. 321–324, 2017.
- [47] R. R. Jha and A. Dubey, "Network-level optimization for unbalanced power distribution system: Approximation and relaxation," *IEEE Transactions on Power Systems*, vol. 36, no. 5, pp. 4126–4139, 2021.
- [48] F. Geth and H. Ergun, "Real-value power-voltage formulations of, and bounds for, three-wire unbalanced optimal power flow," *arXiv preprint arXiv:2106.06186*, 2021.
- [49] T. Akbari and M. Tavakoli Bina, "Linear approximated formulation of AC optimal power flow using binary discretisation," *IET Generation, Transmission & Distribution*, vol. 10, no. 5, pp. 1117–1123, 2016.
- [50] S. Park, R. Y. Zhang, J. Lavaei, and R. Baldick, "Uniqueness of power flow solutions using monotonicity and network topology," *IEEE Transactions on Control of Network Systems*, vol. 8, no. 1, pp. 319–330, 2020.
- [51] C. Wang, A. Bernstein, J.-Y. Le Boudec, and M. Paolone, "Explicit conditions on existence and uniqueness of load-flow solutions in distribution networks," *IEEE Transactions on Smart Grid*, vol. 9, no. 2, pp. 953–962, 2018.
- [52] R. A. Jabr, "High-order approximate power flow solutions and circular arithmetic applications," *IEEE Transactions on Power Systems*, vol. 34, no. 6, pp. 5053–5062, 2019.
- [53] N.-C. Yang and H.-C. Chen, "Decomposed newton algorithm-based three-phase power-flow for unbalanced radial distribution networks with distributed energy resources and electric vehicle demands," *International Journal of Electrical Power & Energy Systems*, vol. 96, pp. 473–483, 2018.
- [54] D. R. R. Penido, L. R. de Araujo, S. Carneiro, J. L. R. Pereira, and P. A. N. Garcia, "Three-phase power flow based on four-conductor current injection method for unbalanced distribution networks," *IEEE Transactions on Power Systems*, vol. 23, no. 2, pp. 494–503, 2008.
- [55] K. Christakou, J.-Y. LeBoudec, M. Paolone, and D.-C. Tomozei, "Efficient computation of sensitivity coefficients of node voltages and line currents in unbalanced radial electrical distribution networks," *IEEE Transactions on Smart Grid*, vol. 4, no. 2, pp. 741–750, 2013.
- [56] K. Alzaareer, M. Saad, H. Mehrjerdi, H. M. Al-Masri, A. Q. Al-Shetwi, D. Asber, and S. Lefebvre, "New voltage sensitivity analysis for smart distribution grids using analytical derivation: ABCD model," *International Journal of Electrical Power & Energy Systems*, vol. 137, p. 107799, 2022.
- [57] R. T. Marler and J. S. Arora, "The weighted sum method for multi-objective optimization: new insights," *Structural and multidisciplinary optimization*, vol. 41, no. 6, pp. 853–862, 2010.
- [58] M. A. Gennert and A. L. Yuille, "Determining the optimal weights in multiple objective function optimization," in *ICCV*, 1988, pp. 87–89.
- [59] Irish Social Science Data Archive. (2012), "Commission for energy regulation (CER) smart metering project," [Online], <http://www.ucd.ie/issda/data/commissionforenergyregulationcer/>.
- [60] C. Wang, G. Song, P. Li, H. Ji, J. Zhao, and J. Wu, "Optimal siting and sizing of soft open points in active electrical distribution networks," *Applied energy*, vol. 189, pp. 301–309, 2017.
- [61] M. L. Bynum, G. A. Hackebeil, W. E. Hart, C. D. Laird, B. L. Nicholson, J. D. Sirola, J.-P. Watson, and D. L. Woodruff, *Pyomo—optimization modeling in python*, 3rd ed. Springer Science & Business Media, 2021, vol. 67.
- [62] B. Bixby, "The gurobi optimizer," *Transp. Re-search Part B*, vol. 41, no. 2, pp. 159–178, 2007.
- [63] Supplementary materials, "Dataset settings of networks in case study," [Online], <https://github.com/cuixueyuan/Network-parameters>.
- [64] W. Kersting, "Radial distribution test feeders," *IEEE Transactions on Power Systems*, vol. 6, no. 3, pp. 975–985, 1991.
- [65] F. Bu, Y. Yuan, Z. Wang, K. Dehghanpour, and A. Kimber, "A time-series distribution test system based on real utility data," in *2019 North American Power Symposium (NAPS)*. IEEE, 2019, pp. 1–6.
- [66] R. F. Arritt and R. C. Dugan, "The IEEE 8500-node test feeder," in *IEEE PES T&D 2010*, 2010, pp. 1–6.
- [67] R. Cheng, Z. Wang, Y. Guo, and Q. Zhang, "Online voltage control for unbalanced distribution networks using projected Newton method," *IEEE Transactions on Power Systems*, vol. 37, no. 6, pp. 4747–4760, 2022.
- [68] B. C. de Souza, L. R. de Araujo, and D. R. R. Penido, "Multi-area aggregation of multi-grounded unbalanced distribution systems," *IEEE Transactions on Power Systems*, vol. 36, no. 6, pp. 5120–5130, 2021.
- [69] X. Zhou, Z. Liu, C. Zhao, and L. Chen, "Accelerated voltage regulation in multi-phase distribution networks based on hierarchical distributed algorithm," *IEEE Transactions on Power Systems*, vol. 35, no. 3, pp. 2047–2058, 2020.



Xueyuan Cui received the B.E. and M.S. degrees from Zhejiang University, Hangzhou, China, in June 2019 and March 2022, respectively, both in electrical engineering. He is currently a Ph.D. student with the Department of Electrical and Electronic Engineering, The University of Hong Kong. His research interests include power system operation and network balancing technologies.



science and machine learning applications.

Guangchun Ruan (Member, IEEE) received the Ph.D. degree in electrical engineering from Tsinghua University in 2021. He is currently a postdoc with the Laboratory for Information & Decision Systems (LIDS) at Massachusetts Institute of Technology (MIT). Before joining MIT, he was a postdoc with the University of Hong Kong in 2022, a visiting scholar with Texas A&M University in 2020, and a visiting scholar with the University of Washington in 2019. His research interests include electricity markets, energy resilience, demand response, data



François Vallée received the degree in civil electrical engineering and the Ph.D. degree in electrical engineering from the Faculty of Engineering, University of Mons, Belgium, in 2003 and 2009, respectively. He is currently a Professor and leader of the “Power Systems and Markets Research Group” at University of Mons. His Ph.D. work has been awarded by the SRBE/KBVE Robert Sinave Award in 2010. His research interests include PV and wind generation modeling for electrical system reliability studies in presence of dispersed generation.



decision-making in modern power systems.

Jean-François Toubeau received the degree in civil electrical engineering, and the Ph.D. degree in electrical engineering, from University of Mons (Belgium) in 2013 and 2018, respectively. He was a postdoctoral researcher of the Belgian Fund for Research (F.R.S/FNRS) within the “Power Systems and Markets Research Group” of University of Mons. He is currently a postdoctoral researcher within the “Energy Systems Integration & Modeling Group” of KU Leuven (Belgium). His research mainly focuses on bridging the gap between machine learning and



The University of Hong Kong. His research interests include data analytics in smart grids, energy forecasting, multi-energy systems, Internet-of-things, cyber-physical-social energy systems.

Yi Wang (Member, IEEE) received the B.S. degree from Huazhong University of Science and Technology in June 2014, and the Ph.D. degree from Tsinghua University in January 2019. He was a visiting student with the University of Washington from March 2017 to April 2018. He served as a Postdoctoral Researcher in the Power Systems Laboratory, ETH Zurich from February 2019 to August 2021.

He is currently an Assistant Professor with the Department of Electrical and Electronic Engineering,